






Chapter 7



Cenozoic Evolution of the Sierra Nevada de Santa Marta, Colombia

<https://doi.org/10.32685/pub.esp.37.2019.07>

Published online 26 November 2020

Mauricio PARRA^{1*} , Sebastián ECHEVERRI² , Ana María PATIÑO³ , Juan Carlos RAMÍREZ⁴ , Andrés MORA⁵, Edward R. SOBEL⁶, Ariel ALMENDRAL⁷, and Andrés PARDO-TRUJILLO⁸ 

Abstract The highest coastal relief on Earth occurs in the Sierra Nevada de Santa Marta in northern Colombia. With an average elevation of ca. 4 km and peaks up to ca. 5.8 km, this small mountain range lies only 85 km to the south of an abyssal plain ca. 3.5 km deep in the Caribbean Sea. A compilation of sparse bedrock and detrital low-temperature thermochronometric data, new detrital apatite fission-track and apatite (U–Th)/He data from modern river sediments, and stratigraphic patterns of adjacent Miocene – Pliocene basins document episodic tectonic development of the Sierra Nevada de Santa Marta. A Paleocene collision of oceanic crust with western Colombia triggered initial exhumation and westward monoclinical tilting of the formerly contiguous Central Cordillera and Santa Marta Massif. Subsequent late Eocene (ca. 35 Ma) dismembering of both ranges occurred associated with right-lateral translation of the Caribbean Plate against the northwestern continental margin of Colombia. This episode marked the onset of contrasting exhumation histories, characterized by low denudation and pediment formation in the Central Cordillera and rapid, episodic exhumation of the Santa Marta Massif, associated with normal faulting and opening of extensional basins along its southwestern margin. Multiple approaches to extracting exhumation rates from thermochronometry, including 1D and 3D reconstructions, reveal that following rapid late Eocene – early Miocene rock uplift, asymmetric exhumation characterized the Sierra Nevada. On the southwestern margin, moderate to rapid exhumation favored progradation of alluvial fan deposits on top of shallow marine and fan delta facies. In contrast, diminished exhumation prompted a reciprocal stratigraphy in the northern margin, where facies retrograde, leading to the accumulation of shallow marine facies on fan delta and alluvial fan deposits. Thermochronometric ages of outcropping units retrieved from modern river sands imply a very recent (<2 Ma) pulse of exhumation, possibly triggered by removal of lower crust, whose precise magnitude and time constraints remain unknown.

Keywords: *Sierra Nevada de Santa Marta, Caribbean Plate, thermochronology, sediment provenance.*

Resumen El mayor relieve topográfico costero de la Tierra ocurre en la Sierra Nevada de Santa Marta en el norte de Colombia. Con una elevación promedio de ca. 4 km y picos de hasta ca. 5,8 km, esta pequeña cordillera yace tan solo 85 km al sur de una

- 1 mparra@iee.usp.br
Universidade de São Paulo
Instituto de Energia e Ambiente
Av. Professor Luciano Gualberto 1289, Cidade Universitária
São Paulo, Brasil
 - 2 juanesecheverri@gmail.com
Universidade de São Paulo
Instituto de Geociências
Rua do Lago 562, Cidade Universitária
São Paulo, Brasil
 - 3 anamariapta@gmail.com
Universidade de São Paulo
Instituto de Geociências
Rua do Lago 562, Cidade Universitaria
São Paulo, Brasil
 - 4 ramirezjuanc11@yahoo.com
Universidade de São Paulo
Instituto de Geociências
Rua do Lago 562, Cidade Universitaria
São Paulo, Brasil
 - 5 andres.mora@ecopetrol.com.co
Ecopetrol S.A
Vicepresidencia de Exploración
Bogotá, Colombia
 - 6 ed@geo.uni-potsdam.de
Instiut fuer Erd- und Umweltwissenschaften
Karl Liebnicht Str 25, 14476
Potsdam, Germany
 - 7 ariel.almendral.vazquez@nr.no
Norwegian Computing Center
P.O. Box 114 Blindern
NO-0314 Oslo, Norway
 - 8 andres.pardo@ucaldas.edu.co
Universidad de Caldas
Instituto de Investigaciones en Estratigrafía
Manizales, Colombia
- * Corresponding author

Supplementary Information:

S1: <https://www2.sgc.gov.co/LibroGeologiaColombia/tgc/sgcpubesp37201907s1.pdf>

S2: <https://www2.sgc.gov.co/LibroGeologiaColombia/tgc/sgcpubesp37201907s2.pdf>

Citation: Parra, M., Echeverri, S., Patiño, A.M., Ramírez, J.C., Mora, A., Sobel, E.R., Almendral, A. & Pardo-Trujillo, A. 2020. Cenozoic evolution of the Sierra Nevada de Santa Marta, Colombia. In: Gómez, J. & Mateus-Zabala, D. (editors), The Geology of Colombia, Volume 3 Paleogene – Neogene. Servicio Geológico Colombiano, Publicaciones Geológicas Especiales 37, p. 185–213. Bogotá. <https://doi.org/10.32685/pub.esp.37.2019.07>

llanura abisal de ca. 3,5 km de profundidad en el mar Caribe. La compilación de los pocos datos existentes de termocronología de baja temperatura, tanto de roca del basamento como detríticos; nuevos datos detríticos de trazas de fisión y (U-Th)/He en apatitos en sedimentos activos y el estudio estratigráfico de cuencas marginales miocenas–pliocenas adyacentes documentan una evolución tectónica episódica de la Sierra Nevada de Santa Marta. La colisión paleocena de corteza oceánica contra el margen occidental de Colombia desencadenó el levantamiento inicial y el basculamiento monoclinial hacia el oeste de un cinturón contiguo formado por la cordillera Central y el Macizo de Santa Marta. El posterior desmembramiento de estas dos cordilleras en el Eoceno tardío (ca. 35 Ma) ocurrió asociado a la translación dextral lateral de la Placa del Caribe a lo largo del margen continental noroccidental de Colombia. Este episodio marcó el inicio de historias contrastantes de desarrollo orogénico, caracterizadas por bajas tasas de denudación y desarrollo de pedimento en la cordillera Central y exhumación rápida y episódica en la Sierra Nevada de Santa Marta, asociada a fallamiento normal y apertura de cuencas extensionales en su margen suroccidental. Múltiples métodos para calcular tasas de exhumación a partir de termocronología, incluyendo modelado 1D y 3D, sugieren que tras un episodio de levantamiento rápido en el Eoceno tardío–Mioceno temprano se presentó exhumación asimétrica en la Sierra Nevada. En el margen suroccidental, la exhumación moderada a rápida favoreció la progradación de abanicos aluviales sobre depósitos marinos someros y facies de deltas en abanico. Por el contrario, una disminución en las tasas de levantamiento generó un patrón de apilamiento estratigráfico opuesto en el margen norte, en donde las facies retrogradaron, lo que causó la acumulación de facies marinas someras sobre depósitos de abanicos aluviales y deltas en abanico. Las edades termocronométricas de las rocas aflorantes obtenidas en sedimentos activos de barras fluviales revelan un pulso muy reciente (<2 Ma) de exhumación, posiblemente asociado a la remoción de corteza inferior, y cuya magnitud y temporalidad precisas aún están por descubrir.

Palabras clave: *Sierra Nevada de Santa Marta, Placa del Caribe, termocronología, procedencia sedimentaria.*

1. Introduction

Oblique convergence and dextral shearing along the northwestern South American margin since the Late Cretaceous have shaped one of the areas with highest topographic relief on Earth in the Sierra Nevada de Santa Marta (SNSM) (Figure 1). Although recent investigations have revealed key episodes concerning the kinematics of early orogenic stages along this margin, the timing and associated driving mechanisms for Cenozoic uplift of the SNSM remain elusive. Sparse but relatively old (>15 Ma) low-temperature mineral cooling ages (Cardona et al., 2011a; Villagómez et al., 2011) and a positive gravity anomaly in the SNSM (Figure 1a) have been used to suggest that the range is in a stage of denudational immaturity, that is, recent crustal stacking and rock uplift exceed the magnitude of exhumation (Parra et al., 2016; Villagómez et al., 2011), portraying a case of non-steady state topography likely due to a young pulse of orogenesis.

Here, we summarize the uplift record and Cenozoic tectonic evolution of the SNSM based on geochronologic, thermochronologic, and stratigraphic data. We present and update

published data as well as summarize new results that portray a two-stage uplift history and an E–W asymmetry and pose new hypotheses regarding the mechanisms driving episodic rock uplift and exhumation during the Cenozoic.

2. Geological Setting

The Cenozoic tectonic evolution of the northwestern margin of South America has been controlled by the interactions of the Caribbean and Pacific Oceanic Plates with the continental margin and the attendant stages of ocean terrane accretion, magmatic growth, tectonic deformation, and sedimentary basin formation (Bayona et al., 2012; Duque-Caro, 1984; Gorney et al., 2007; Kellogg, 1984; Mann et al., 2006; McMahon, 2000; Montes et al., 2015; Pindell et al., 1998).

In the northernmost Andes of Colombia, the along-strike continuity of the Andean chain is replaced by a series of discontinuous uplifted massifs surrounded by Cenozoic basins. Such fragmentation has been associated with the eastward migration of the Caribbean Plate since the Eocene. One such massif is the SNSM, a triangular pyramidal, fault-bounded, basement block

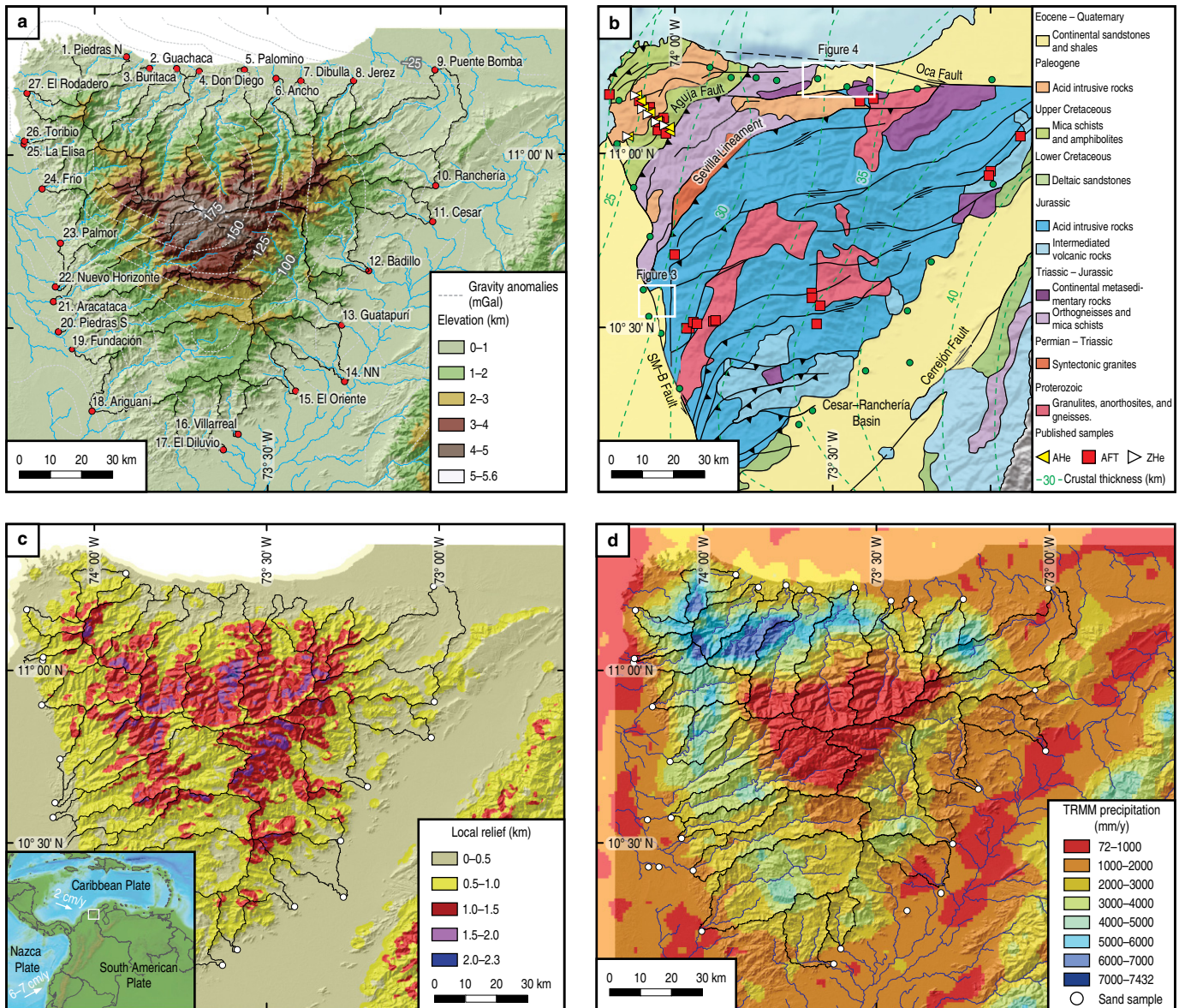


Figure 1. Morphotectonic configuration of the SNSM. **(a)** SRTM 90 topography, Bouguer gravity anomalies (white lines) and location of new detrital thermochronometric samples collected in active river bars and their drainage areas. **(b)** Simplified geologic map (after Tschanz et al., 1969) showing the location of published bedrock thermochronometric samples and values of crustal thickness (after Yarce et al., 2014). White squares denote the areas shown in Figures 3, 4. (SM-B Fault) Santa Marta-Bucaramanga Fault **(c)** Local relief in a 3 km-diameter circular window. Inset map shows the bottom topographic and plate velocities (after Trenkamp et al., 2002). **(d)** Tropical Rainfall Measuring Mission (TRMM) precipitation data (Mulligan, 2006).

isolated between Cenozoic basins in the humid, northwestern corner of the Maracaibo Microplate (Figure 1a, 1d; Burke et al., 1984; Cediél et al., 2003). The range's structural boundaries are the right-lateral Oca Fault in the north and the left-lateral Santa Marta-Bucaramanga Fault in the west, which in addition to a neotectonic strike-slip character (Idárraga-García & Romero, 2010) has an important vertical displacement that has generated the range's structural relief (Figure 1c) and controlled the sedimentation in adjacent basins since the Oligocene. To the east, the serranía de Perijá thrusts along El Cerrejón Fault onto the SNSM basement buried beneath ca. 2.5 km of clastic strata in

the Cesar-Ranchería Basin (Kellogg & Bonini, 1982; Montes et al., 2010).

The SNSM Massif exposes igneous and metamorphic basement rocks of Proterozoic, Permian – Triassic, Triassic – Jurassic, Cretaceous, and Paleocene – Eocene ages (Cardona et al., 2006, 2010a, 2010b, 2011b; Cordani et al., 2005; Duque, 2010; Restrepo-Pace et al., 1997; Tschanz et al., 1969). These rocks are grouped into three geological provinces bounded by SW-NE-striking, subparallel reverse fault systems with NW vergence (Figure 1b; Tschanz et al., 1974): (1) To the southeast, the Sierra Nevada province occupies

more than two-thirds of the SNSM area and consists of an ensialic basement made up of high-grade metamorphic rocks of Grenvillian age (1.0–1.2 Ga; Cardona et al., 2010a; Case & MacDonald, 1973; Tschanz et al., 1974), intruded by undeformed Jurassic – Lower Cretaceous acid plutonic rocks and covered by felsic volcanic rocks of Jurassic age (Cardona et al., 2006); (2) Underthrust beneath the Sierra Nevada province along the Sevilla Fault lies the Sevilla province, made up of an ensialic basement of medium- and low-grade metamorphic rocks (amphibolites and micaceous schists) of Paleozoic age (Cardona et al., 2006; Tschanz et al., 1974; Weber et al., 2009), intruded by Permian – Triassic syntectonic granitoids (Cardona et al., 2010b); (3) Farther to the northwest, the Sevilla province overthrusts an imbricate series of Late Cretaceous – Paleocene allochthonous terranes of Caribbean affinity along the Aguja Fault. They comprise the Santa Marta province, metamorphosed to greenschist to amphibolite facies during an accretionary event along the continental margin in the Late Cretaceous – Paleocene, and made up of a series of low- to middle-grade metavolcanic–sedimentary rocks and orthogneisses arranged in SW–NE-oriented belts. Paleocene to Eocene granitoids (e.g., the Buritaca, Latal, and Toribio Plutons) intruded into both the Santa Marta and Sevilla provinces (Cardona et al., 2011b; Duque, 2010; Salazar et al., 2016; Tschanz et al., 1974) constrain the age of collision between late Maastrichtian and early Paleocene (Cardona et al., 2010c).

Basement correlations from the SNSM (Cardona et al., 2010b) across the Plato–San Jorge and the Lower Magdalena Basins (Ceron et al., 2007; Montes et al., 2010; Mora–Bohórquez et al., 2017) to the Central Cordillera (Ordóñez–Carmona & Pimentel, 2002; Restrepo et al., 2011; Vinasco et al., 2006) support the view of a contiguous Late Cretaceous – Paleocene belt including the Central Cordillera and the SNSM. Tectonic isolation of this ancestral range is thought to have resulted from post–Eocene escape tectonics associated with dextral migration of the Caribbean Plate (e.g., Pindell & Kennan, 2009), generating ca. 30° vertical-axis clockwise rotation (Montes et al., 2010) or a mixture between rotation and translation (Reyes et al., 2004). Such dextral movement led to simultaneous extension in the Ariguani, Plato, and San Jorge Sub-basins along the southwestern segment (Lower Magdalena Basin) and contraction in the Cesar–Ranchería Basin to the east (Bayona et al., 2010; Montes et al., 2010).

Due to the preservation of strata as young as Miocene in the basins surrounding the SNSM, most of the vertical displacement associated with the Santa Marta–Bucaramanga and Oca Faults is thought to be late Cenozoic in age (Case & MacDonald, 1973). However, older exhumation is supported by late Paleocene and Eocene apatite fission-track ages along the southeastern margin of the range (Villagómez et al., 2011; see section 5.1), as well as by provenance data for Paleogene

strata in the Cesar–Ranchería Basin suggesting an active source area in the Central Cordillera–SNSM (Ayala et al., 2009, 2012; Bayona et al., 2007). Eocene to recent exhumation patterns in the SNSM based on geobarometry and fission-track and (U–Th)/He thermochronology (Cardona et al., 2011a) document peak magnitudes of basement exhumation of ca. 15–19 km in the northwestern range’s corner and decreasing magnitudes toward the SE, so that cooling ages become older (and therefore average exhumation rates lower; see section 5.2). This southward decrease in the magnitude of exhumation has been explained as the result of large-scale clockwise monoclinical tilting that finally results in net basement burial beneath up to ca. 2.2 km of clastic strata in the Cesar–Ranchería Basin (Montes et al., 2010; Sánchez & Mann, 2015).

A positive total Bouguer gravity anomaly of ca. 200 mGal exists in the SNSM (Figure 1a; e.g., Agencia Nacional de Hidrocarburos, 2010) and has been interpreted to reflect (1) the absence of a crustal root due to lack of isostatic compensation (e.g., Case & MacDonald, 1973; Kellogg & Bonini, 1982) or (2) underplating of an abnormally thick oceanic slab that resists subduction (Ceron, 2008).

3. Stratigraphy

The sedimentary archives hosting the SNSM’s ancient denudation are preserved in isolated Cenozoic basins associated with normal and left–lateral movement of the Bucaramanga Fault and right–lateral movement of the Oca Fault on the SW and N sides of the range, respectively (Figure 1b). Tschanz et al. (1969) coined the names Guajira Trough and Riohacha for the northern basins and Ariguani Trough for the western basin and provided a generalized description of their sedimentary fill. These pioneering works and other stratigraphic studies and geologic mapping at scales of 1:100 000 and 1:25 000 for the western and northern foothills of the SNSM (e.g., Colmenares et al., 2007; Hernández et al., 2003; Piraquive et al., 2017; Tschanz et al., 1969) have produced a series of maps and stratigraphic profiles using different stratigraphic nomenclatures. However, the absence of robust chronostratigraphic control generates problems of synonymy, definition, and stratigraphic correlations (e.g., Hernández et al., 2003; Piraquive et al., 2017). A summary of chronostratigraphic correlations is presented in Figure 2 and associated references.

3.1. Ariguani Trough

Toward the eastern border of the Lower Magdalena Basin (LMB), the transcurrent movements of the Santa Marta–Bucaramanga and Algarrobo Faults generated a pull-apart basin with up to 7–8 km of sediment thickness preserved, as documented by seismic, gravimetric, and magnetometric data (Bernal–Olaya et al., 2015; Mora et al., 2018; Reyes et al.,

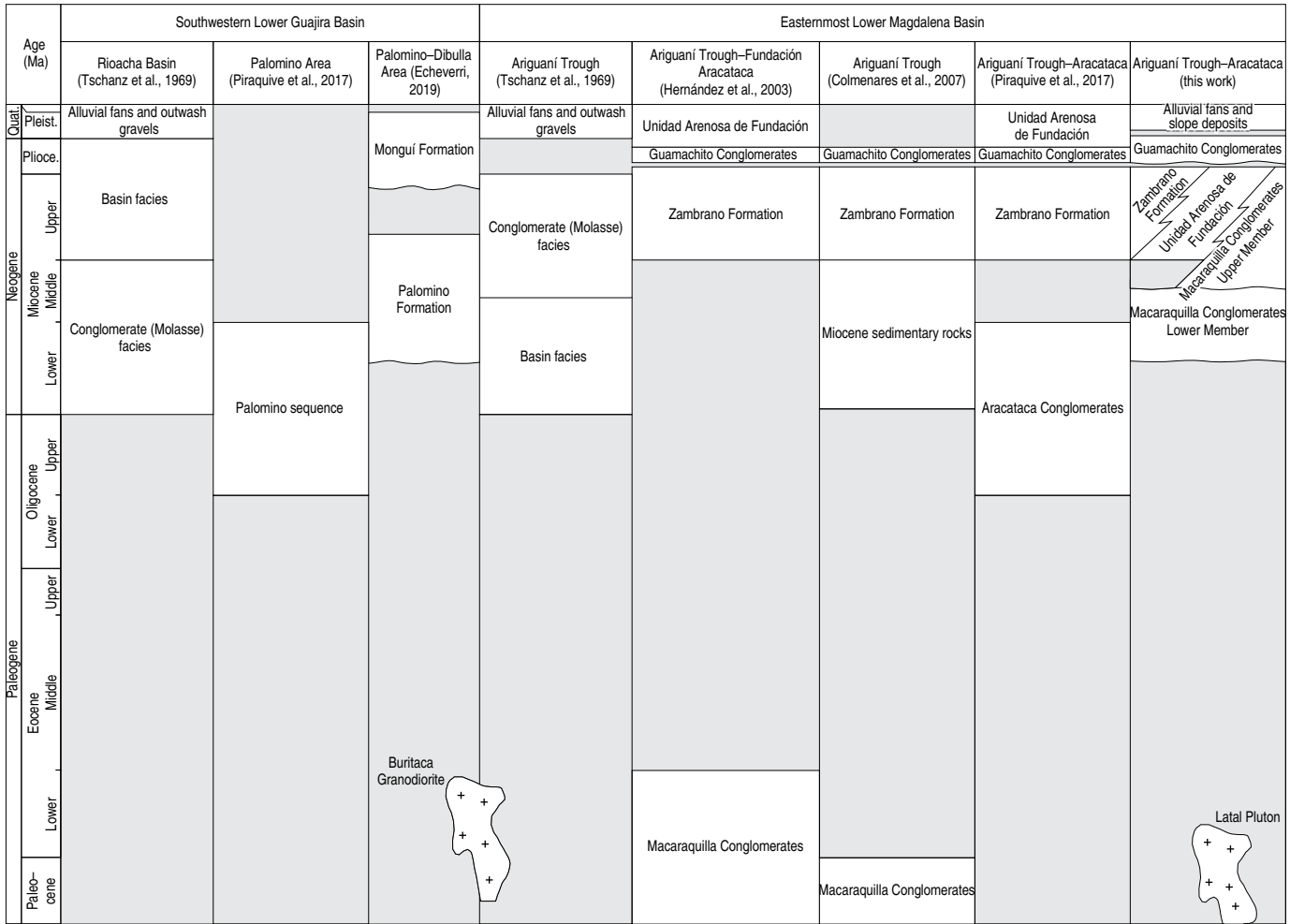
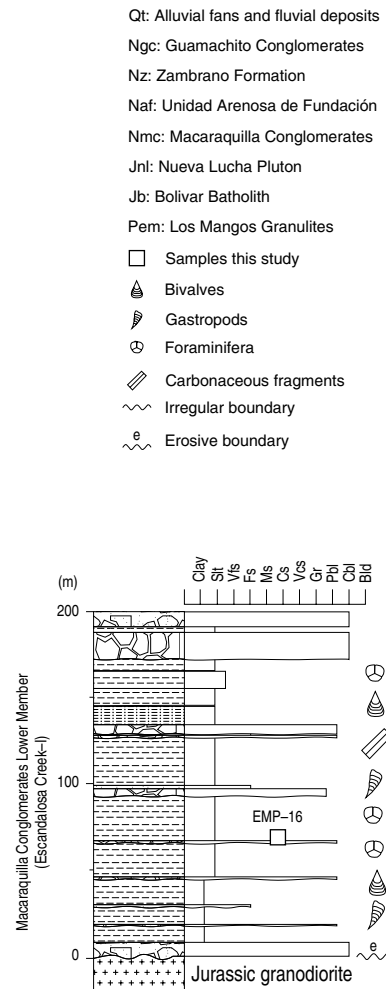
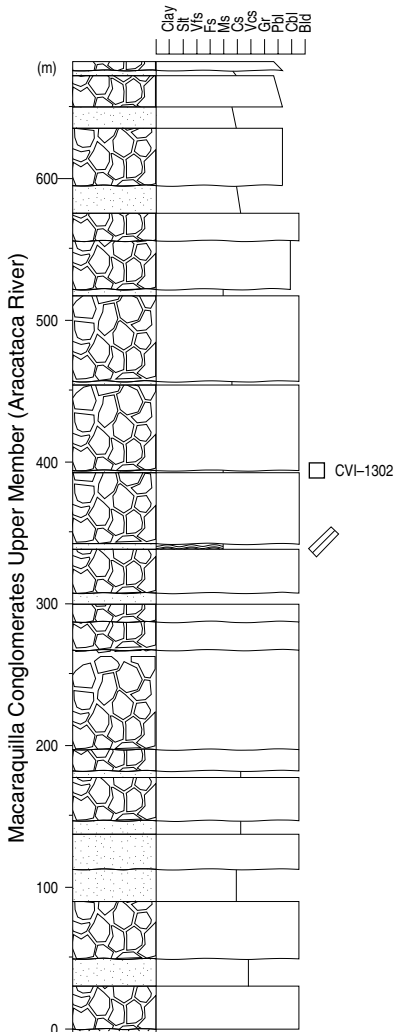
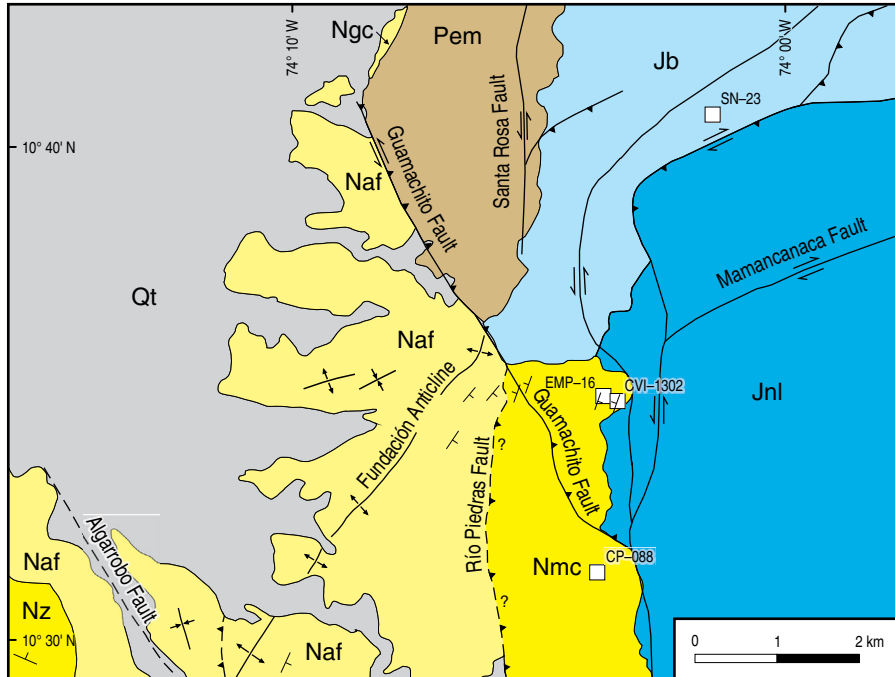
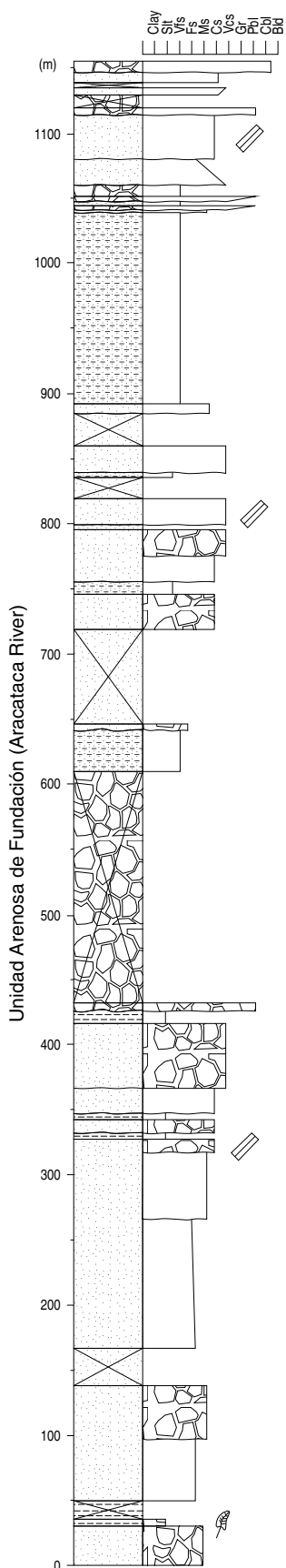


Figure 2. Chronostratigraphic chart of the Lower Guajira and Ariguani Basins.

2004). The fault activity probably began in the early Oligocene, as suggested by correlations with the basal sedimentary strata of the Plato Sub-basin (Rincón et al., 2007), but the age of the oldest sedimentites in the depocenter of the Ariguani Trough remains unknown. Stratigraphic correlations with the lowermost strata found in a structural high to the west in the Alagorobo-1 well (Rincón et al., 2007) suggest a minimum age of late Oligocene.

The basal strata of this succession are exposed in the western foothills of the SNSM and are limited to the west by the Río Piedras reverse fault (Figure 3; Colmenares et al., 2007). They consist of a west-dipping, dominantly conglomeratic unit (Macaraquilla Conglomerates; Hernández et al., 2003), ca. 1250 m thick (Pinzón-Rodríguez, 2014) and consisting of two members that nonconformably overlie either Jurassic intermediate to acid granitoids or the Precambrian Los Mangos Granulite. Sediment accumulation has been interpreted to have occurred in fan deltas sourced by the SNSM (Piraquive

et al., 2017) and has been assigned, without any chronostratigraphic foundation, to either the Paleocene – Eocene (Hernández et al., 2003) or the Oligocene – early Miocene (Piraquive et al., 2017). However, previous accounts based on inconclusive macrofossils tentatively suggest a Miocene age (Tschanz et al., 1969). West of the Río Piedras Fault, Hernández et al. (2003) identify two lithostratigraphic units exposed along the limbs of the Fundación Anticline: (1) The Zambrano Formation, as described in areas west of the city of Fundación, consists of at least 500–800 m of interbedded sandstones (some of them bioclastic), marls, and mudstones, and accumulated in shallow marine and lagoonal environments in the late Miocene – early Pliocene, according to palynologic data (Hernández et al., 2003); (2) At least 500 m of dominantly coarse- and medium-grained sandstones, variegated mudstones, and thin pebble conglomerates of interpreted estuarine origin have been informally named the “Unidad Arenosa de Fundación”. Based on a faulted contact against the Macaraquilla Conglom-



- Qt: Alluvial fans and fluvial deposits
- Ngc: Guamachito Conglomerates
- Nz: Zabrano Formation
- Naf: Unidad Arenosa de Fundación
- Nmc: Macaraquilla Conglomerates
- Jnl: Nueva Lucha Pluton
- Jb: Bolivar Batholith
- Pem: Los Mangos Granulites
- Samples this study
- 🐚 Bivalves
- 🐌 Gastropods
- 🌀 Foraminifera
- ▨ Carbonaceous fragments
- ~ Irregular boundary
- ⤴ Erosive boundary



Figure 3. Geologic map (modified after Colmenares et al., 2007) and composite stratigraphic section of the Ariguani Basin in the western margin of the SNSM.

erates and on the age of the Zambrano Formation, Hernández et al. (2003) assigned a Pliocene age. As shown below (section 5.1), and indicated in Figures 2 and 3, we reinterpret the stratigraphic succession based on our new lithostratigraphic and biostratigraphic observations and group the strata cropping out in the western sector of the Río Piedras Fault's footwall into the Unidad Arenosa de Fundación. The Guamachito Conglomerates constitute the uppermost unit preserved in the Aracataca Trough. It consists of coarse-grained clastic facies made up of matrix-supported polymictic pebble and cobble conglomerates with plutonic clasts up to 1 m in diameter, medium- to coarse-grained lithic micaceous sandstones, and mudstones containing plant remains, and its provenance was assigned by Tschanz et al. (1969), without further details, to the SNSM. The lower contact is erosive and unconformable with the Zambrano Formation, which has led Hernández et al. (2003) to assign a stratigraphic age of Pliocene – Pleistocene to the Guamachito Conglomerates.

3.2. Lower Guajira Basin

North of the SNSM, the Guajira Trough Basin is part of the southwestern extent of the Lower Guajira Basin (Figure 4) and is structurally limited by major basement uplifts brought to the surface along major faults configuring a flat topography where surface outcrops are limited. It hosts north-dipping siliciclastic sedimentary fill consisting of two main facies: (1) To the south of the Oca Fault, the so-called Palomino sequence (Piraquive et al., 2017) is a succession of cobble conglomerates, conglomeratic sandstones, and lithic sandstones with minor sandy variegated mudstones with uncertain thickness, ranging from measured 500 m (Piraquive et al., 2017) to inferred 2400 m (Tschanz et al., 1969). The unit nonconformably overlies Jurassic and Eocene granitoids or is in faulted contact against these granitoids or older Precambrian metamorphic units (Colmenares et al., 2007) and has been interpreted as a nearshore deposit, possibly estuarine. No age constraints have been provided for this unit, but a Miocene age has been inferred due to the stratigraphic position (Piraquive et al., 2017). (2) North of the Oca Fault, the Mongui Formation is a mudstone-dominated succession made up of variegated claystones, some of which are fossiliferous, and fine- to medium-grained sandstones, most likely several thousand meters thick (Tschanz et al., 1969). No age constraints are available onshore, but a stratigraphic correlation based on the projection to the south of biostratigraphically dated subsurface strata from seismic lines in Cadena & Slatt (2013) supports a Pliocene age.

4. Materials and Methods

Here, we present a tectonic evolution history of the SNSM based on published and new thermochronometric data, both bedrock and detrital, and new stratigraphic and provenance data from surrounding basins. Low-temperature thermochronometry is the study of the thermal history of rocks as they cool below ca. 250 °C, based on the study of isotopic systems that involve the accumulation of radiogenic decay products, either fission-tracks (e.g., Gallagher et al., 1998; Tagami & O'Sullivan, 2005) or helium nuclei (Farley, 2002; Harrison & Zeitler, 2005) due to spontaneous decay of U and Th isotopes. These radiogenic products are effectively accumulated in a mineral crystal lattice only at low temperatures. Above a threshold temperature, solid-state diffusion and track annealing occur faster than the rates of daughter production associated with radioactive decay, precluding their accumulation. Rather than at a specific temperature, the thermal loss of radiogenic daughter products occurs in a temperature range that has been called the partial retention zone (e.g., Reiners & Brandon, 2006). The concept of closure temperature is a mathematical approximation of a temperature within this range that usefully describes the thermal sensitivity of thermochronometric systems considering monotonic cooling only (Dodson, 1973). For the (U–Th)/He system in apatite (AHe), this closure temperature is ca. 70 °C for nondamaged crystals (Farley, 2002) but can be as high as ca. 120 °C for heavily radiation-damaged apatites (Flowers et al., 2009; Gautheron et al., 2009). For the apatite fission-track (AFT) system, this temperature varies between 100 and 140 °C, depending mainly on apatite composition and solubility (e.g., Donelick et al., 2005; Gallagher et al., 1998).

We present a new dataset consisting of (1) six bedrock AFT ages and (2) detrital data from AFT and AHe collected in sand bars of 3 modern rivers. Analytical details for these new analyses are presented in the Supplementary Information 1. We further present published fission-track and (U–Th)/He data in apatite and zircon (AFT, AHe, ZFT, and ZHe, respectively) from igneous and metamorphic rocks collected across the SNSM, most of them from an elevation profile in the range's northwestern corner, others from an elevation profile in the western slope, and few additional data from the northern and eastern slopes. In addition, we include a new analysis of existing detrital data collected in Miocene strata in the northern and western margins (Piraquive et al., 2017).

Based on these combined data, which constitute all available low thermochronometric data from the SNSM, we first extract

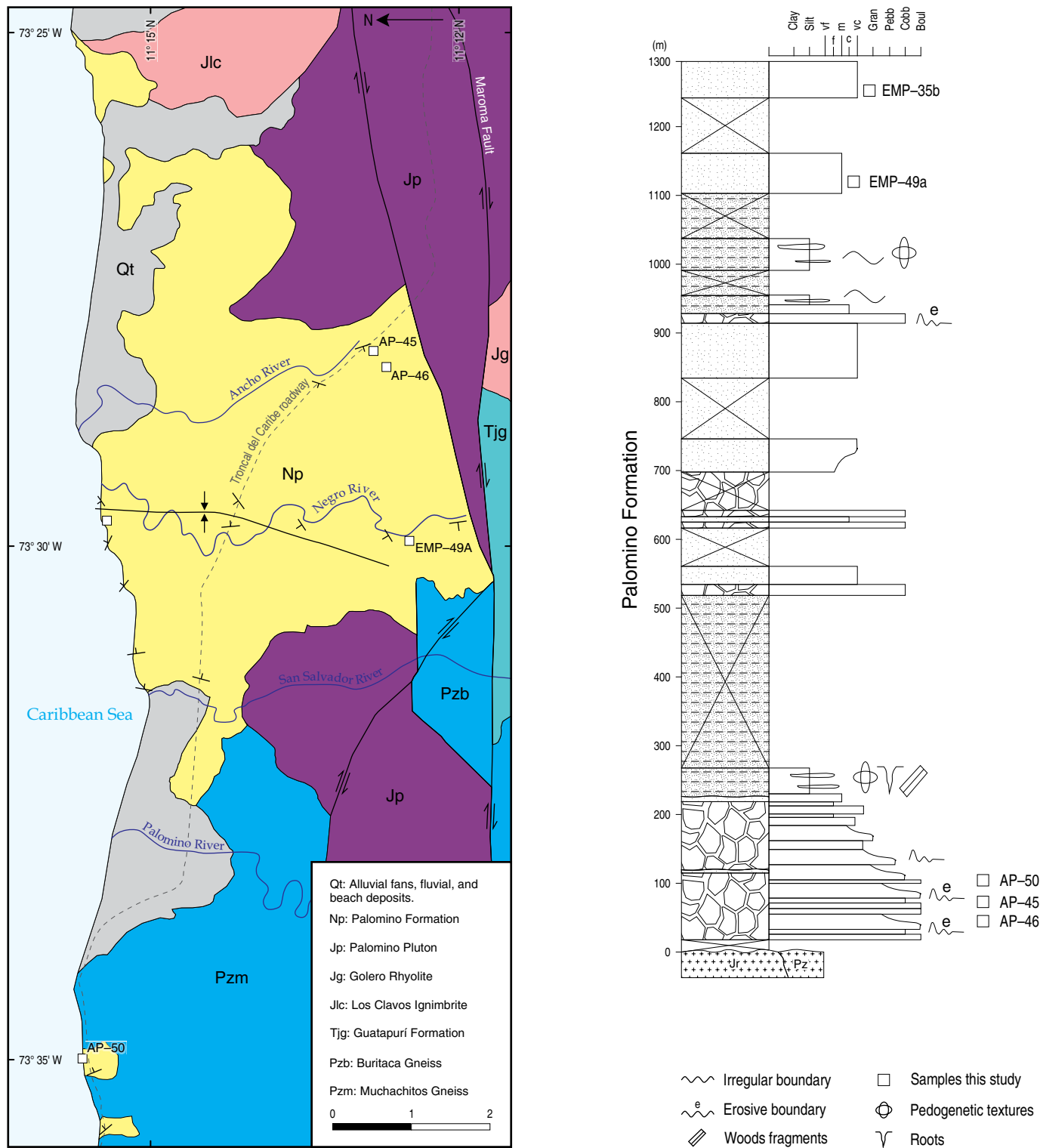


Figure 4. Geologic map (modified after Colmenares et al., 2007) and composite stratigraphic section of the Lower Guajira Basin in the northern margin of the SNSM.

long-term exhumation rates based on a simplified 1D approach that consists of using the youngest cooling age peaks for each particular thermochronometric system as the approximate age for the passage of rocks across the isotherms of 70 °C, 120 °C, and 250 °C, corresponding to average closure temperatures for

the AHe, AFT, and ZFT systems, respectively, and calculate the associated magnitude of exhumation using geothermal gradients of 20–25 °C/km, an acceptable range for retroarc foreland basins (e.g., Allen & Allen, 2005), and a surface temperature of 20 °C. Exhumation rates are thus calculated by dividing the

magnitude of exhumation by the time span between intervening isotherms. We further explore plausible thermotectonic histories that are consistent with bedrock and detrital data through 3D thermokinematic modeling of these combined data using the software Pecube (Braun, 2003; Braun et al., 2012) in order to extract long-term exhumation rates.

Finally, we present new structural and stratigraphic cross-cutting relationships, new biostratigraphic data based on palynomorphs (see Supplementary Information 1), and summarize recent stratigraphic observations that reveal hints about the ages and mechanisms of concurrent basement exhumation and basin formation.

5. Results

5.1. Stratigraphy

Our stratigraphic surveying in the eastern limb of the Fundación Anticline reveals that the Macaraquilla Conglomerates disconformably overlies granitoids with paleo-regolith fabrics (Figure 5a, 5b) of an assigned Jurassic age (Colmenares et al., 2007). The basal sequence exhibits contrasting lithofacies across a NW-dipping fault: to the SE, in the footwall block, the basal facies consists of a ca. 1 m-thick layer of lithic arkosic sandstones overlain by massive grayish sandy mudstones, whereas to the west, they consist of matrix-supported conglomerates containing cobbles and boulders of the Jurassic substratum (Figure 5b). These field relationships document that sediment accumulation occurred concomitant with normal faulting. In a stratigraphic section measured in the footwall block, the Macaraquilla Conglomerates comprises two members. The Lower Member consists of ca. 220 m of fossiliferous siltstones and interlayered marls, limestones, scarce lithic arkosic sandstones, and oligomictic and polymictic conglomerates. Marls and fossiliferous siltstones contain abundant bivalves, gastropods, and wood fragments (Figure 5c). The Upper Member of the Macaraquilla Conglomerates is constituted by a monotonous succession of ca. 900 m-thick, polymictic conglomeratic beds with a few interlayers of coarse-grained, lithic arkosic sandstones (Figure 5c). Heterolithic facies of siltstones and bioturbated sandstones with carbonaceous sheets occur sporadically. Sandstones include heavy minerals such as garnet, clinopyroxene, and hornblende. Southwesterly paleocurrents based on imbricated clast measurements and other provenance data based on sandstone and conglomerate petrography unequivocally document provenance from the SNSM (Echeverri et al., 2017; Piraquive et al., 2017).

We report here the occurrence of spores of *Nijssenosporites fossilatus* (Figure 5c) in samples SNT-93A and SNT-88 from the Lower and Upper Members, respectively, and of pollen *Zonocostites ramonae*, which allow assigning a maximum age of early Miocene, based on the zonation of Jaramillo et al. (2011).

Our observations and published data (Piraquive et al., 2017) suggest that this stratigraphic succession records sediment progradation through a change in sedimentary environments from marine–transitional to deltaic and alluvial environments (Echeverri et al., 2017; Piraquive et al., 2017).

Toward the western segment of the Aracataca River, in the eastern limb of the Fundación Anticline, the Upper Member of the Macaraquilla Conglomerates exhibits an interdigitated to transitional contact with the distal Unidad Arenosa de Fundación (sensu Hernández et al., 2003). The upper limit is defined by either the actual erosive surface or by unconformably overlying Quaternary alluvial fans and slope deposits in the Aracataca River area (Figure 3). The Unidad Arenosa de Fundación thus represents a sandstone-dominated unit laterally equivalent to the Upper Member of the Macaraquilla Conglomerates. This unit has a stratigraphic thickness of ca. 1450 m and consists of medium- to very coarse-grained lithic arkosic sandstones alternating with sporadic intercalations of siltstones and conglomerates. Sandstones display thick and very thick layers with tabular, wavy, and lenticular geometry and massive, gradational, or laminated internal structures. Conglomerates appear as medium and thick layers, sporadically very thick, with lenticular and tabular geometry and massive internal structure, in some segments with imbricated clasts. Carbonized woody remnants and dicotyledonous cuticles are frequent in this unit. This interval records southwesterly paleocurrents and indicates provenance from the SNSM (Echeverri et al., 2017), registering a progradation of sedimentary environments from the platform-prodelta to fluvial and deltaic sedimentation (Echeverri et al., 2017; Hernández et al., 2003; Tschanz et al., 1969).

5.2. Bedrock Thermochronometry

Published bedrock thermochronometry from the SNSM (Figure 6) includes a total of 27 apatite fission-track (AFT) data, mainly collected along two elevation profiles, one in the Sierra Nevada province at the range's western margin (Figure 6b; Fundación profile, 10 samples; Villagómez et al., 2011) and one in the northwestern corner of the Santa Marta province (Figure 6c, 6d; Kennedy profile, 11 samples). AFT ages (2-sigma error) range from 23.3 ± 4.4 Ma to 53.8 ± 8.2 Ma in the Fundación profile and from 16.0 ± 2.5 Ma to 41.0 ± 9.6 Ma in the Kennedy profile, in both cases with relatively good age–elevation correlations. An additional few AFT ages come from a Jurassic granitoid in between the two profiles (26.7 ± 3.6 Ma), from granitoids at the range's northern margin (2 samples, 22.3 ± 3.1 Ma and 27.6 ± 4.6 Ma, from Paleocene and undetermined age, respectively), and from Jurassic granitoids and felsic volcanic rocks at its northeastern margin (3 samples, 40.4 ± 5.7 Ma to 59.6 ± 10.4 Ma) (Figure 6a). In addition, 15 apatite and 14 zircon (U–Th)/He (AHe and ZHe, respectively) single grain ages were obtained from 8 samples along the Kennedy profile, with

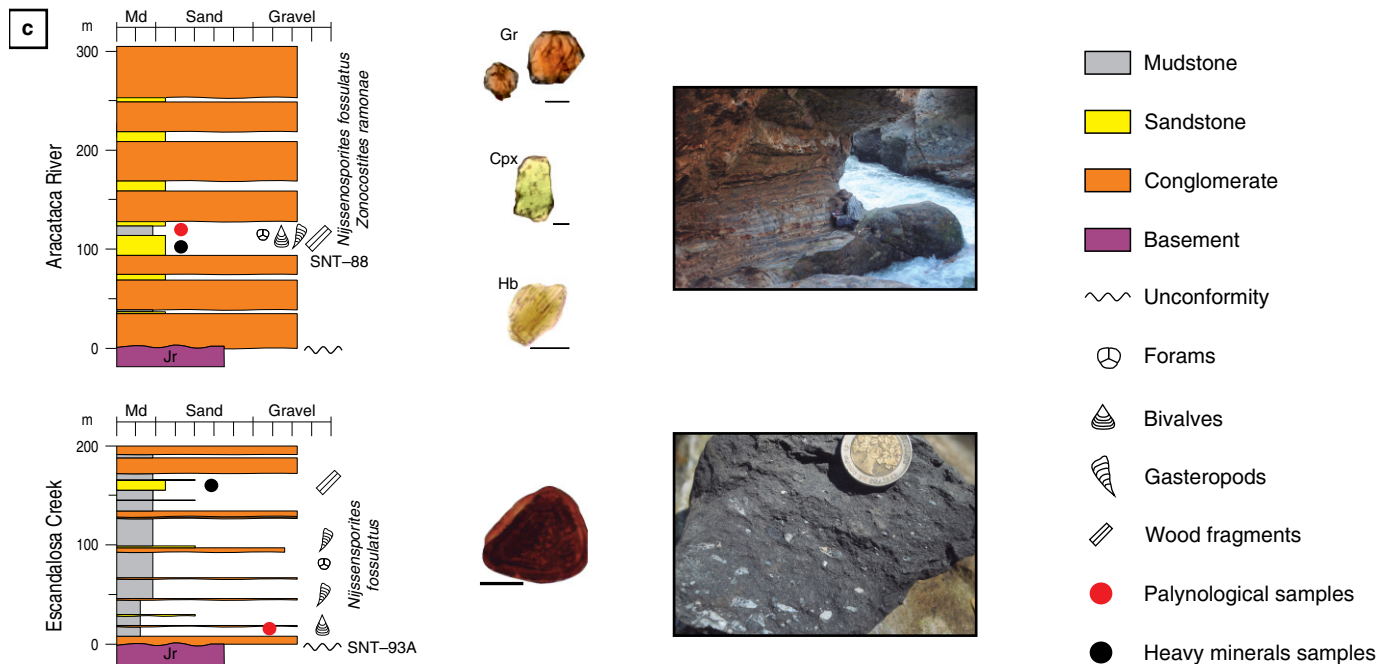
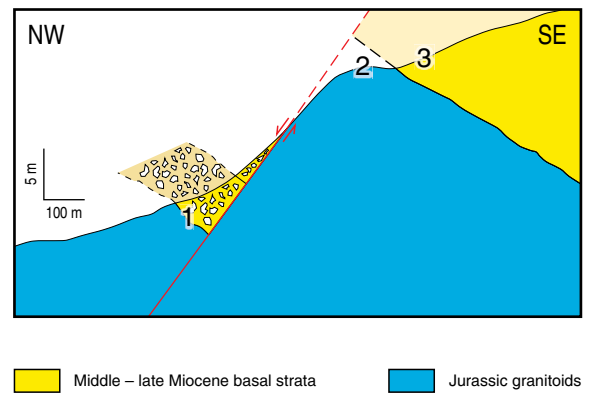
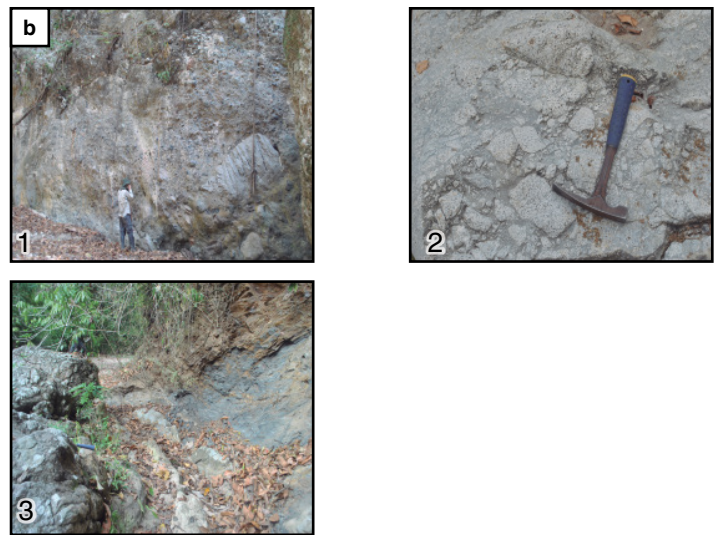
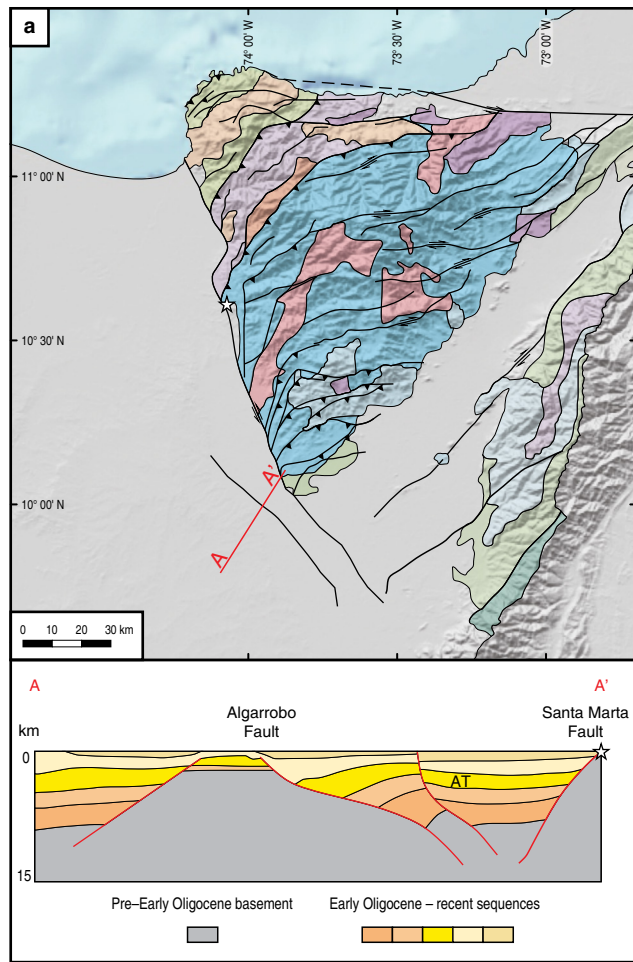


Figure 5. Stratigraphic relationships associated with Miocene synextensional sediment accumulation in the Ariguani Trough. **(a)** Simplified map of the SNSM and localization of the seismic section A–A' in the northeastern LMB, showing the Ariguani Trough (AT) and other depocenters associated with post-Oligocene extension (redrawn after Mora et al., 2018). **(b)** Sketch of geologic section along Escandalosa Creek (location marked by white stars on map and its projection on section A–A') showing a normal fault separating two domains with contrasting basal Cenozoic facies overlying Jurassic granitoids with paleo-regolith fabrics (Picture 2); to the west, in the hanging wall block, boulder conglomerates composed of the underlying substrata (Picture 1) contrast with sandstones and mudstones (Picture 3) in the footwall block to the SE. **(c)** Summarized stratigraphic sections from the Escandalosa Creek and the Aracataca River (see location in Figure 3), showing the characteristic palynomorphs and heavy minerals, identified with mollusk-rich marls (lower picture) and cobble conglomerates (upper picture). (Hb) hornblende; (Cpx) clinopyroxene; (Gr) garnet.

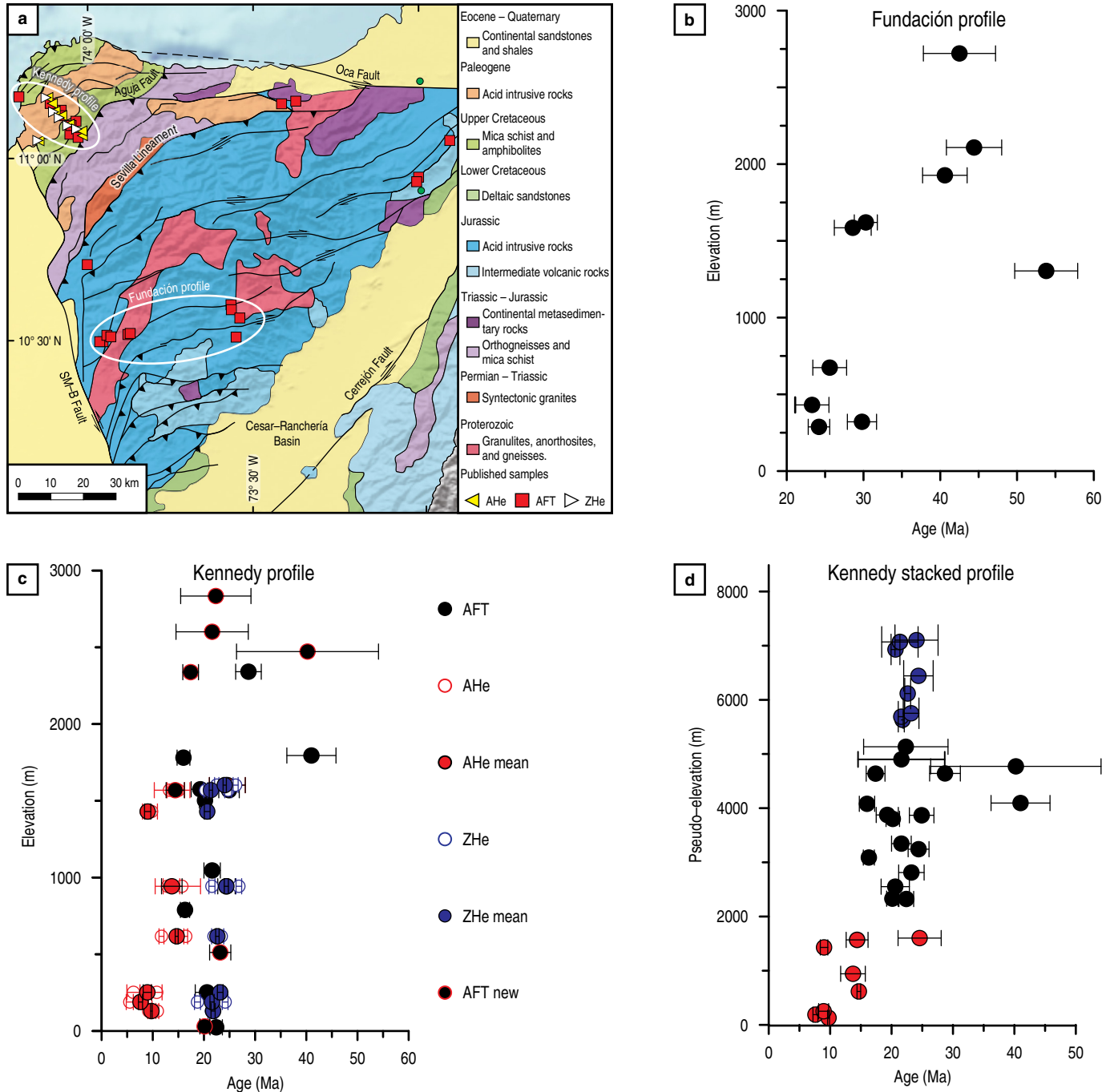


Figure 6. Bedrock thermochronometry. **(a)** Geologic map showing the locations of published thermochronometric samples (Cardona et al., 2011a; Villagómez et al., 2011). **(b), (c)** Age–elevation relationships along the Fundación and Kennedy profiles. **(d)** Age vs. pseudo-elevation (stacked profile) in the Kennedy profile.

good within-sample reproducibility and a fair to good age–elevation relationship (Figure 6d; Cardona *et al.*, 2011a). The weighted averaged AHe ages range from 7.6 ± 0.8 Ma to 24.5 ± 7.0 Ma and ZHe ages from 20.6 ± 0.6 Ma to 24.3 ± 0.5 Ma.

Here, we present new AFT results from 6 additional granitoid, amphibole gneiss, and mica schist samples from the uppermost and lowermost reaches along the Kennedy profile (Figure 6c), as well as from 2 samples of granitoids collected at lower elevations. Despite the few grains available for dating in the two samples at highest elevations (three to six grains, samples SNT-14 and SNT-16), ages over an elevation difference of ca. 250 m are indistinguishable within uncertainty (2σ up to 60%), varying between ca. 21 and 23 Ma (Figure 6d; Table 1). Sample SNT-18 yields an older age with a large uncertainty (40.2 Ma), which we ascribe to very low U contents in the apatites. The two lowermost samples yield less uncertain ages between 20.1 ± 1.9 Ma and 23.2 ± 4.1 Ma, which fit with the trend of data from similar elevations analyzed by Villagómez *et al.* (2011) (Figure 6c).

Collectively, all published and new ages reveal a pattern of younging ages in a northwestward direction, suggesting gradually increasing exhumation rates toward the northwest. In addition, the patterns of ages versus elevation and pseudoelevation (stacked profiles and closure depths estimated as in Reiners & Brandon, 2006) for both elevation profiles document an episode of rapid exhumation between ca. 35 and 15 Ma (Figure 6d). Extracting exhumation rates with this 1D approach is an oversimplification, as it involves assumptions that are violated in nature, such as that isotherms are horizontal and time invariant. However, using 2σ error-weighted linear regressions, we calculate a rate of 0.25 ± 0.09 km/my (between ca. 30 and 15 Ma) for the Kennedy stacked profile and of 0.13 ± 0.08 km/my for the Fundación profile (from 30–20 Ma), which represent minimum values for actual rates (for further explanation, see Braun, 2002).

5.3. Detrital Thermochronometry

Published detrital AFT and ZFT data are available for Cenozoic strata from the northern (Lower Guajira) and western (Ariguaní) margins of the range (Piraquive *et al.*, 2017), assigned to the middle Miocene – Pliocene and early – middle Miocene, respectively, based on regional stratigraphic correlations and the new biostratigraphic data presented here. In the north, AFT data collected in one sample from middle Miocene – Pliocene rocks reveal two AFT age populations of ca. 27 Ma and ca. 53 Ma (Figure 7; see Table 1 of the Supplementary Information 2), implying lag times (i.e., the difference between the thermochronometric age and the stratigraphic age [10 ± 5 Ma, in this case], which represents the time of exhumation from the closure depth; Ruiz *et al.*, 2004) of ca. 11–22 Ma and 38–48 Ma. ZFT detrital ages in 5 samples from the same strata collected along

two stratigraphic sections yield age populations of 33–41 Ma, ca. 55 Ma, 74–90 Ma, 108–132 Ma, 156–170 Ma, and 254 Ma (Figure 8; see Table 1 of the Supplementary Information 2). From these data, we interpret that only the two youngest populations may reflect reset ages related to the Cenozoic Andean cycle of exhumation. Despite the large uncertainties derived from both poorly constrained stratigraphic ages and large errors in cooling age populations, the youngest AFT and ZFT detrital populations help furnish rough estimates of long-term denudation rates. For the following calculations (Table 2), we use mean closure temperatures of 120 °C and 250 °C for the AFT and ZFT systems, respectively, geothermal gradients of 20–25 °C/km, and a time-invariant surface temperature of 20 °C, chosen to represent an average temperature above sea level. The AFT lag-time of ca. 12–22 Ma reveals a maximum Miocene exhumation rate of ca. 0.2–0.4 km/my (4–5 km of exhumation between 27 and 15–5 Ma), preceded by slightly faster rates of 0.4–1.1 km/my (Figure 9; Table 2; 65–6.5 km of exhumation between 41–33 and 27 Ma). In the western margin (Aracataca), a similar analysis derived from strata that we document here as early – middle Miocene in age (see section 5.1) is based on 2 AFT samples with age peaks of 19–22 Ma, 30 Ma, and 42–60 Ma and 3 ZFT samples with age peaks of 29 Ma, 48–52 Ma, 74 Ma, 104–108 Ma, and 167 Ma (Table 2; see Table 1 of the Supplementary Information 2). The youngest cooling ages imply a shorter AFT lag time of 3–11 Ma, corresponding to a fast early – middle Miocene exhumation rate (up to 0.4–1.8 km/my) from ca. 22 to 19–11 Ma, preceded by rates of up to 0.2–0.7 km/my for the underlying 5–6.5 km of crust during the Oligocene – early Miocene (47–29 to 22 Ma; Figure 9).

We present new AFT and AHe data from modern sands collected in longitudinal bars from three rivers draining the northern (Cañas River), southwestern (Fundación River), and southeastern (Guatapurí River) slopes of the SNSM (Figure 10a; see Table 3 for summary results, and Tables 2–6 of the Supplementary Information 2 for single-grain ages and track-length data). For each individual sample, we conducted analyses on 89–101 individual grains for AFT and 23–30 aliquots for AHe. We present the results as box plots (Figure 10b) and kernel density plots (Figure 10c) with calculated age populations for each sample and thermochronometric system using the automatic unmixing model available in DensityPlotter (Vermeesch, 2012).

AFT data from the three catchments show similar age spectra, dominantly with ages younger than 50 Ma and a few older ages (Figure 10b; Table 3). The age distributions are narrow for the northern and western catchments and slightly broader in the easternmost catchment (Figure 10c). The age spectra display one (Guatapurí) or two (Cañas, Fundación) populations in the fraction younger than 50 Ma, which we interpret as exhumation ages associated with Cenozoic orogenesis, and an additional population of older grains (ca. 69 Ma, ca. 63 Ma, and 85 Ma,

Table 1. New bedrock apatite fission-track data.

Sample	Latitude N	Longitude W	Elevation (m)	Lithology	#Gr ^a	U (ppm)	Rho-S (NS) ^b	Rho-I (NI) ^b	Rho-D (ND) ^c	P(χ^2) (%) ^d	Age (Ma) ^e	$\pm 2 \sigma$ error	Dpar (mm)	$\pm 1 s$
SNT-14	11.112	74.035	2834	Amphibolite	3	9.2	1.024 (11)	28.58 (307)	35.80 (5899)	71%	22.3	13.7	1.68	0.23
SNT-16-1	11.108	74.048	2601	Schist	6	9.0	0.969 (11)	5.815 (66)	7.448 (2670)	64%	21.6	14.1	1.62	0.20
SNT-18	11.104	74.061	2472	Gneiss	6	3.0	0.612 (9)	9.454 (139)	35.76 (5899)	49%	40.2	27.7	1.45	0.21
SNT-19-2	11.107	74.061	2338	Gneiss	28	17.5	1.521 (163)	10.66 (1143)	7.011 (2670)	32%	17.4	3.1	2.11	0.46
SNT-27	11.152	74.126	512	Granodiorite	30	6.7	0.767 (162)	4.586 (965)	7.934 (2798)	30%	23.2	4.1	2.22	2.07
SNT-30	11.226	74.161	30	Granodiorite	28	47.0	4.727 (844)	31.83 (5684)	7.791 (2798)	9%	20.1	1.9	2.73	0.37

^a Number of grains analyzed.

^b Rho-S and Rho-I are the spontaneous and induced tracks density measured, respectively ($\times 105$ tracks/cm²). NS and NI are the number of spontaneous and induced tracks counted for estimating Rho-S and Rho-I, respectively.

^c Rho-D is the induced track density measured in the external mica detector attached to CN2 dosimetry glass ($\times 105$ tracks/cm²). ND is the number of induced tracks counted in the mica for estimating Rho-D.

^d P(χ^2) (%) is the chi-square probability (Galbraith, 1981; Green, 1981). Values greater than 5% are considered to pass this test and represent a single population of ages.

^e Pooled (central) age reported for ages that pass (fail) the χ^2 test.

respectively) that we assume represent ancient exhumation events but partially reset. Among the exhumation ages (i.e., those younger than 50 Ma), the youngest age peak occurs in the western catchment (Fundación River, 16.5 ± 1.2 Ma), whereas the oldest appears in the northern region (Cañas River, 22.5 ± 1.6 Ma). AHe ages exhibit a similar pattern, with catchments in the north and west that display only ages younger than ca. 30 Ma, the western catchment (Fundación) with the youngest ages and an eastern catchment including few outliers of unreset ages as old as ca. 85 Ma. A comparison of eU vs. age (i.e., Flowers et al., 2009) reveals no correlation and thus no evidence of radiation damage controlling the age pattern (Figure 10d). Remarkably, AHe and AFT age signatures, as revealed by box plots and the central tendency (Figure 10b; i.e., second quartile or median of the data set of obtained ages) are very similar to the east (Guatapurí River, 27 and 21 Ma, respectively), whereas they are up to ca. 14 my apart for the northern (Cañas, 27 and 18 Ma, respectively) and western (Fundación, 31 and 17 Ma, respectively) catchments. Using closure temperatures of 70 °C and 120 °C for the AHe and AFT systems, respectively, and geothermal gradients of 20–25 °C/km, the youngest AFT age populations render similar long-term exhumation rates since the early Miocene of 0.2–0.3 km/my for the northern, western, and eastern catchments (Figure 9). Unlike AFT-derived rates, AHe data document long-term asymmetric removal of the up-

permost 2–2.5 km of crust, which has been faster (0.3–0.4 km/my) in the north and west during the last ca. 7 my and much slower (0.10–0.15 km/my) in the eastern margin but integrated since ca. 18 Ma (Figure 9).

Together, detrital thermochronometric data from Miocene strata reveal higher exhumation rates for the northern (Palomino) than for the western (Aracataca) catchments in the Oligocene (and earliest Miocene for the western margin), followed by an opposite pattern of acceleration in exhumation in the west in the early – middle Miocene and a middle – late Miocene deceleration in the north. The comparison of Miocene and modern AFT lag times (Figure 7) shows a subtle increase to values of 15 ± 5 Ma to ca. 20 Ma in the northern face and a marked increase of 4–10 Ma to ca. 17 Ma in the western margin. These data illustrate that following the period of Miocene asymmetric exhumation, rates have decreased ever since across the entire range, yet exhumation continues to be fastest in the western slope, fast in the north, and slower in the eastern margin (Figure 9).

5.4. Thermokinematic Modeling

To obtain a more regionally unified account of exhumation rates across the entire range, we forward modeled 3D topographic and kinematic histories that account for the observed

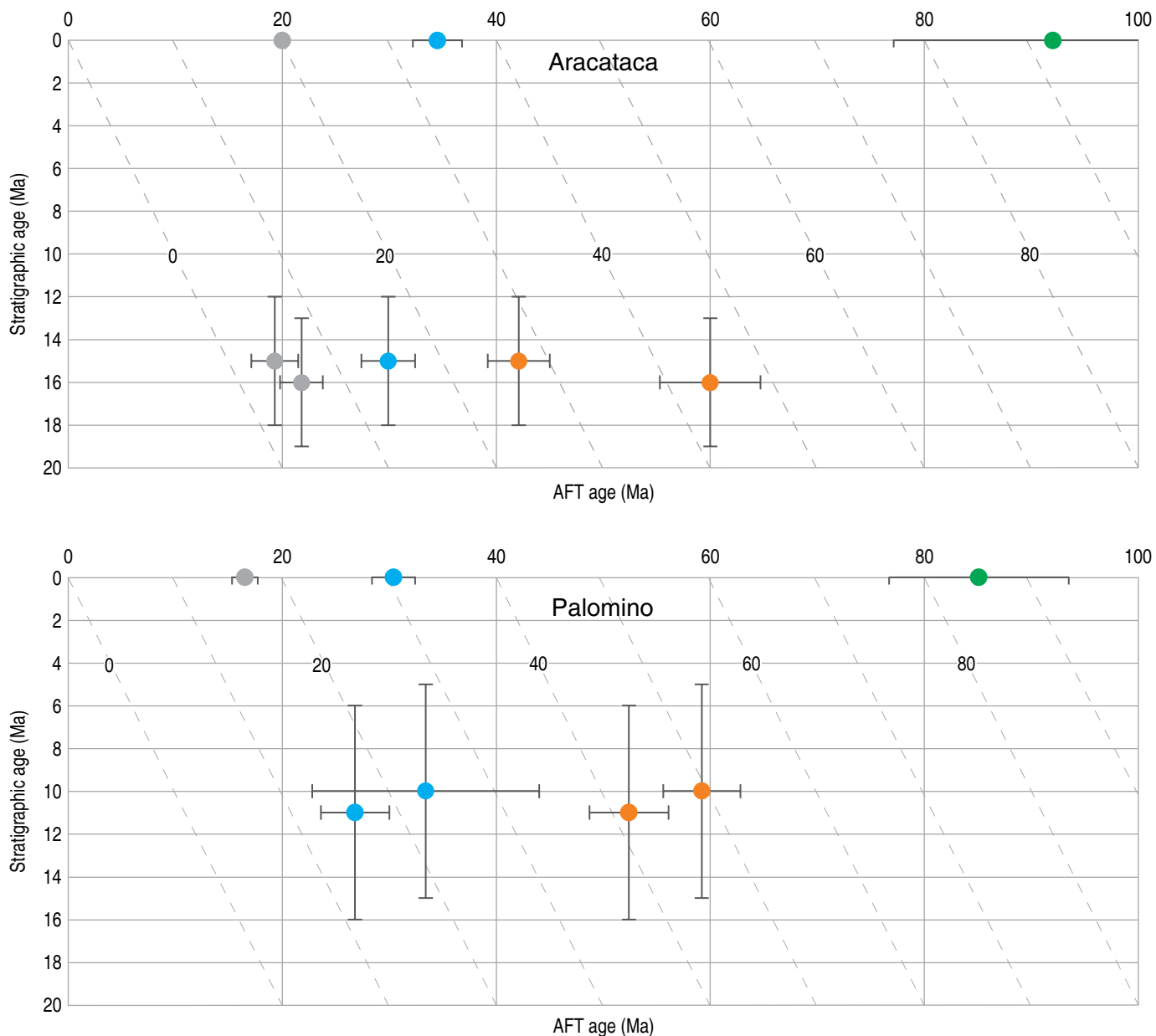
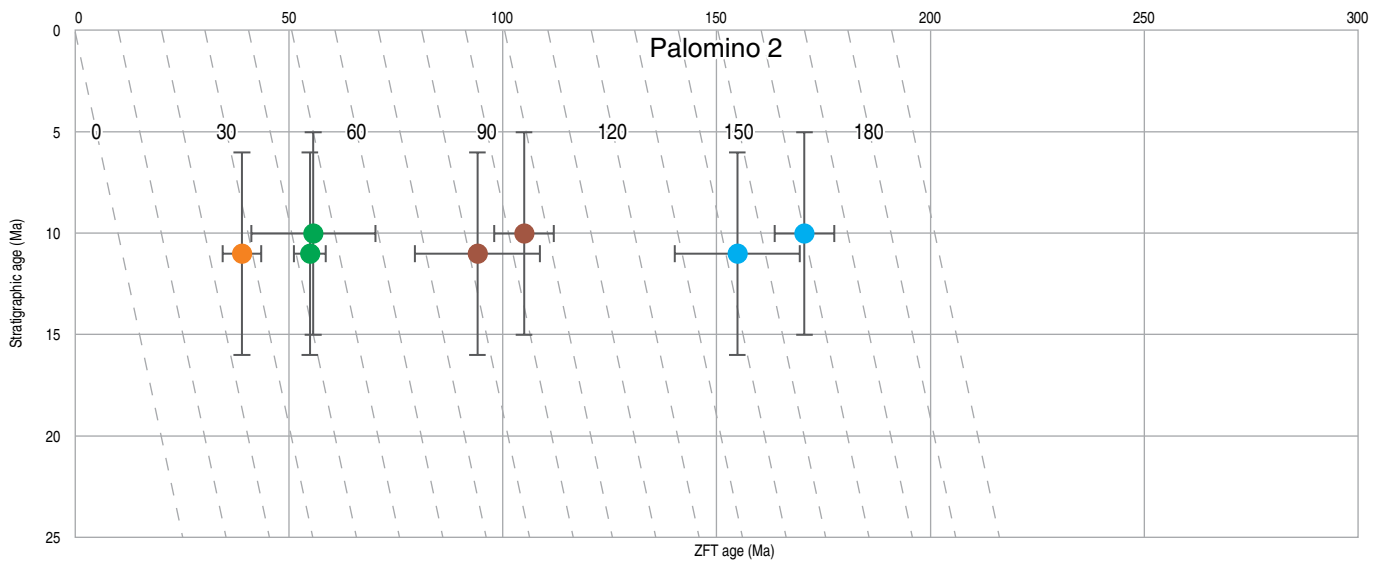
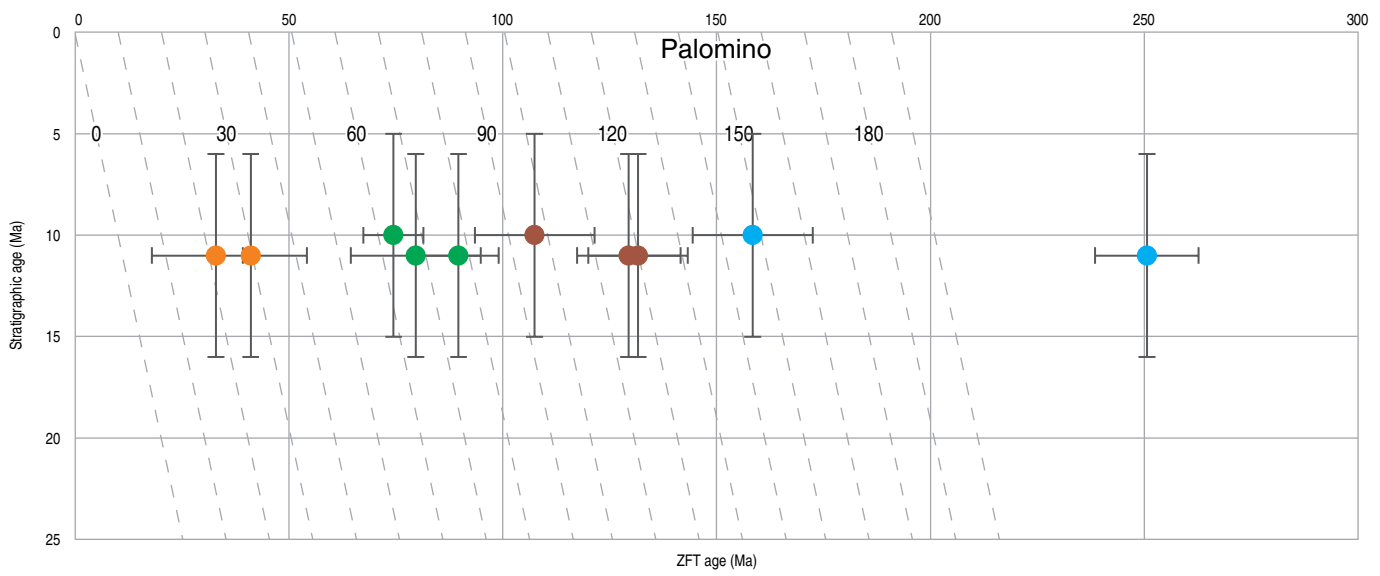
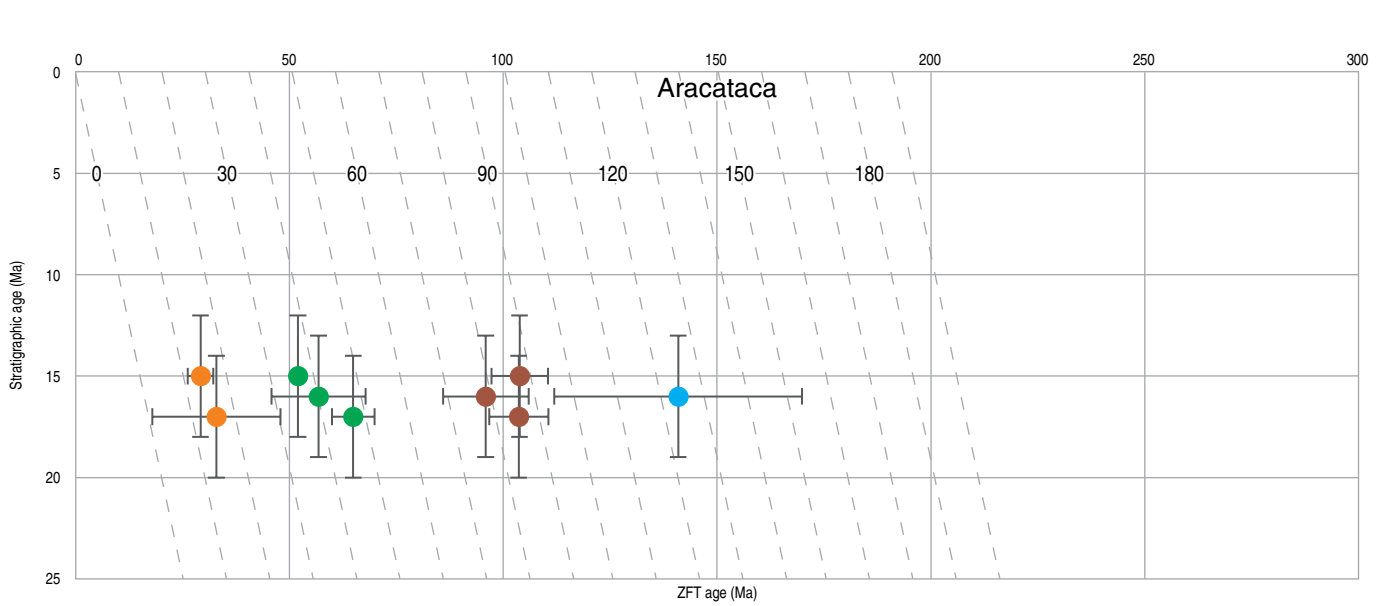


Figure 7. Stratigraphic vs. cooling age plots (lag time plots) for Cenozoic strata in the Aracataca (Ariguaní Trough) and Palomino (Lower Guajira Basin) sections. The inclined lines represent isolines of lag time (i.e., approximate time elapsed between thermochronometric system closure and surface exposure). The figure shows lag time plots for AFT data, representing the approximate time for denudation of the uppermost 4–5 km of rock (between the 120 and 20 °C isotherms). Colored dots represent different populations of detrital ages.

bedrock and detrital thermochronometric data, as well as the structural geometry and asymmetric exhumation, using the software Pecube (Braun, 2003; Braun et al., 2012). Pecube is a numerical model that solves the heat-transfer equation in three dimensions in a crustal block with topographic and fault kinematic evolutions prescribed independently, but in which heat advection is considered to occur only vertically. With such assumptions, this type of thermokinematic

Figure 8. Stratigraphic vs. cooling age plots (lag time plots) for Cenozoic strata in the Aracataca (Ariguaní Trough) and Palomino (Lower Guajira Basin) sections. The inclined lines represent isolines of lag time (i.e., approximate time elapsed between thermochronometric system closure and surface exposure). The figure shows lag time plots for ZFT data, representing the approximate time for erosion of the uppermost 9–11.5 km of rock (between the 250 and 20 °C isotherms). Colored dots represent different populations of detrital ages.



Quaternary
Neogene
Paleogene

Table 2. Youngest detrital AFT and ZFT age populations in Cenozoic strata in the Palomino and Aracataca sections (data from Piraquive et al., 2017) and calculated exhumation rates.

1. AFT peaks and exhumation rates from the 120 °C isotherm to the surface (20 °C).									
Section	Sample	Youngest AFT peak (Ma)	Stratigraphic age (Ma) ^a	Lag-time (my)		Exhumation rates (km/my)			
				min	max	20 °C/km		25 °C/km	
						min	max	min	max
Aracataca (W)	CVI-1302	19.3	15 ± 4	0.3	8.3	16.7	0.6	13.3	0.5
	EMP-16	21.8	15 ± 4	2.8	10.8	1.8	0.5	1.4	0.4
Palomino (N)	AP-045	26.8	10 ± 5	11.8	21.8	0.4	0.2	0.3	0.2

2. ZFT peaks and exhumation rates between the 250 °C and 120 °C isotherms.							
Section	Sample	Youngest ZFT peak (Ma)	Youngest AFT peak (Ma)	Lag-time AFT-ZFT (my)	Exhumation rates (km/my)		
					20 °C/km	25 °C/km	
Aracataca (W)	CVI-1302	29.2	19.3	9.9	0.7	0.5	
	CP-088	47.4	19.3	28.1	0.2	0.2	
Palomino (N)	AP-046	32.9	26.8	6.1	1.1	0.9	
	AP-045	41	26.8	14.2	0.5	0.4	

^a Stratigraphic ages for Aracataca based in our new biostratigraphic data and for Palomino based on stratigraphic position (see discussion in text).

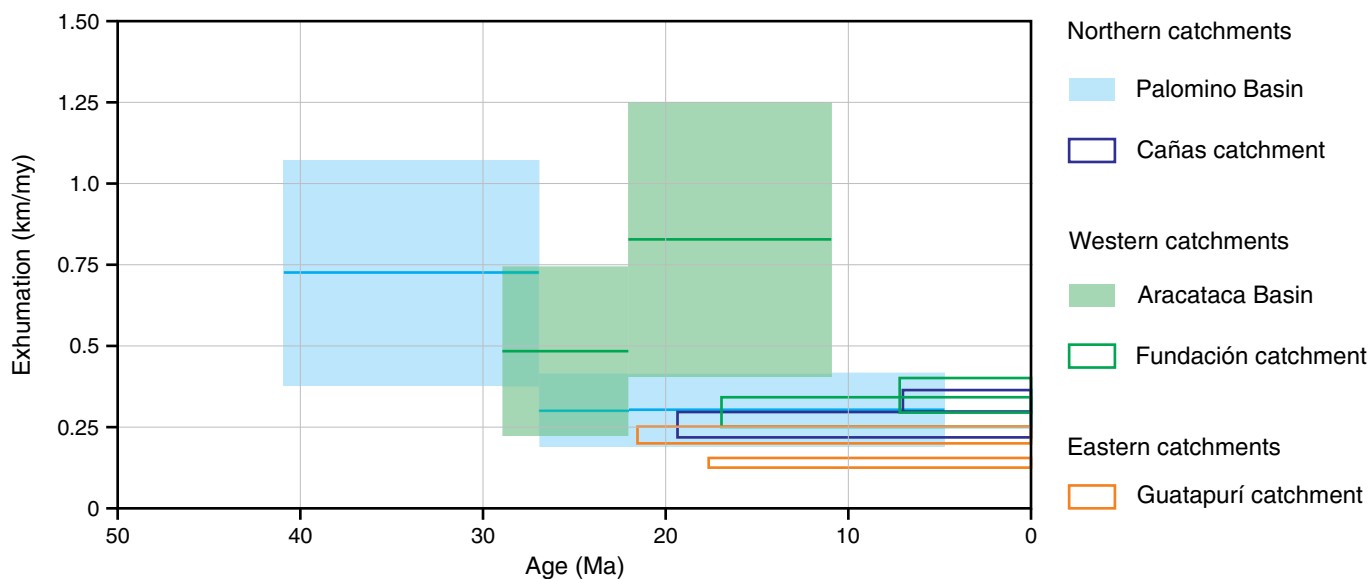


Figure 9. Evolution of Cenozoic exhumation rates estimated with one-dimensional calculations using detrital thermochronometric data from Cenozoic strata and modern sediments. The magnitude of exhumation was estimated using a surface temperature of 20 °C and average closure temperatures of 70 °C, 120 °C, and 250 °C for the AHe, AFT, and ZFT systems, respectively, and a range of geothermal gradients from 20–25 °C/km. The timespan corresponding to the transit of rocks between adjacent isotherms was calculated by subtracting the ages of the corresponding thermochronometric youngest peaks. See the text for further explanation.

modeling is capable of translating a forward modeled kinematic history into a thermal history and, finally, into modeled thermochronometric ages using available kinetic models (i.e., fission-track annealing or He/Ar diffusion in minerals), thereby enabling the comparison of thermochronometric modeled ages

with measured ages and hence allowing the validation of plausible topographic and kinematic scenarios.

In our approach, rather than intending to reliably resolve the kinematics of faulting in the SNSM, we aim at revealing plausible Cenozoic exhumation rates across the range. To ac-

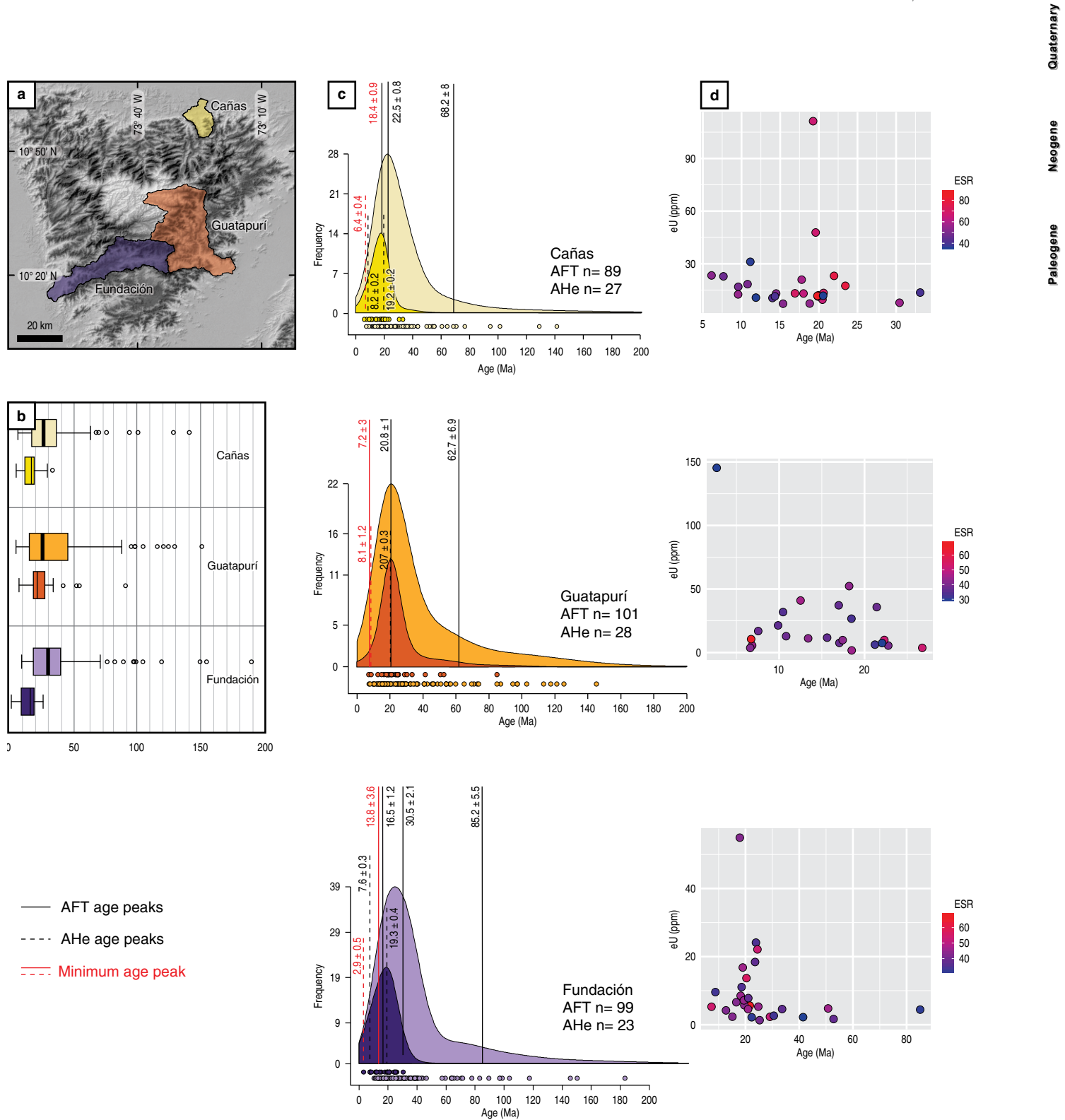


Figure 10. Detrital thermochronometry in selected catchments from the northern (Cañas), western (Fundación), and eastern (Guatapuri) slopes of the SNSM. **(a)** Locations of river catchments. **(b)** Box plots and central tendencies (thick dark lines) for AFT (pale colors) and AHe (dark colors) ages. **(c)** Kernel density plots for AFT (pale colors) and AHe (dark colors). Dots represent individual ages. Thick (dashed) lines and numbers in the upper (lower) part of each plot represent AFT (AHe) age peaks. Red lines and numbers represent the youngest peaks used to calculate integrated maximum exhumation rates. **(d)** Age vs. effective uranium content (eU = $U + 0.235Th$). Each dot represents an individual aliquot and is color-coded based on the aliquot's grain size, reported as the equivalent-sphere radius (ESR).

Table 3. Summary of detrital apatite fission-track and (U–Th)/He data from modern sand samples.

Sample	Latitude N	Longitude W	Elevation (m)	AFT											AHe					
				#Gr ^a	P1 ^b			P2			P3			#Gr ^a	P1			P2		
					Age	2 σ	%	Age	2 σ	%	Age	2 σ	%		Age	2 σ	%	Age	2 σ	%
Cañas	11.211	73.402	29	90	22.5	1.6	81.6	68.2	16.0	18.4				28	8.2	0.2	26.2	19.2	0.3	73.8
Guatapurí	10.506	73.283	237	101	20.8	2.0	73.6	62.7	13.8	26.4				30	20.7	0.3	100.0			
Fundación	10.427	74.031	128	99	16.5	2.4	30.3	30.5	4.2	52.7	85.2	11	17.0	23	7.6	0.3	43.0	19.3	0.8	57.0

^a Number of grains analyzed.

^b P1 to P3 are age populations extracted using the automatic unmixing model implemented in DensityPlotter (Vermeesch, 2012).

count for the observed southeastward monoclinical tilting and the northwestward younging in thermochronometric ages, we chose two kinematic scenarios that simulate a gradient in vertical exhumation rates (Figure 11): (1) a series of NE–striking vertical faults with eastward decreasing velocities and (2) one or multiple southeastward–dipping reverse faults with either ramp–flat or listric geometries and velocities decreasing eastward. For each group of simulations, we departed from a base model with a series of fixed thermal and elastic parameters, as described in Table 4, and systematically modified the geometric, topographic, and kinematic parameters. We ran more than 300 forward Pecube models and for each of them evaluated the misfit between modeled and observed ages, the latter including bedrock AFT and AHe data and detrital data from river sand samples, through the log–likelihood function (LLH). This function describes the plausibility of the model parameters given specific observed data, and its calculation attempts to find an estimate of parameters that maximizes its value (see Supplementary Information 1 for a more detailed description). In short, the LLH calculation yields negative values, so the highest value is the one closest to zero.

5.4.1. Models of Group 1: Southeast–dipping Faults

A first set of models was designed to test the effect of different fault geometries on the vertical exhumation rates. We prescribed a model with one main fault located at the western end of the range, striking parallel to the Aguja and Sevilla Faults, ca. N45°E, and two geometries, listric and a ramp geometry (Figure 11a), and ran simulations using similar topographic evolutions but with different fault velocities since 65 Ma. The better models (i.e., those with higher LLH values, closer to 0) show that the fault slip rates that more suitably reproduce both the AFT and AHe thermochronometric data are 0.20–0.35 km/my (Figure 12a). The results show that either listric geometry reliably reproduces the data, as this geometry is the one that involves a gradient in vertical displacement that is faster in the

western sector of the range. A ramp geometry, which involves uniform vertical displacement along the whole hanging wall, does not adequately reproduce the data. The best model is one with a listric fault with a velocity of 0.32 km/my since 65 Ma. These velocities represent the integrated fault velocities over a period between 65 Ma and the present time. However, AFT data, representing the uppermost 4–5 km of exhumation, are better reproduced with lower velocities, with a range of 0.10–0.20 km/y (Figure 12c), whereas AHe data, representing the erosion of the uppermost 2.0–2.5 km of crust, require faster vertical displacements, of 0.20–0.40 km/my (Figure 12b). Altogether, the modeling results support fault acceleration anytime since the Miocene.

5.4.2. Models of Group 2: Vertical Faults

A second group of models was run imposing a kinematic scenario of vertical displacement only. We chose to reproduce the SW tilting by modeling exhumation with a series of vertical reverse faults also striking N45°E and with fault velocities decreasing eastward, all starting to operate at 65 Ma. We arbitrarily chose 4 faults in order to generate the velocity gradient. The location of the westernmost fault (A) was chosen at the same location as the fault used in the first group of models, and the remaining 3 faults, B, C, and D, were located 25, 30, and 45 km southeastward (Figure 11b). Based on the results of the models with southeast–dipping faults, in which best models with 0.2–0.35 km/my along listric or circular faults set up the maximum vertical velocity, we tested models in which we assumed an initial set of velocities for faults A, B, C, and D and then systematically varied the velocity of each fault, starting with fault A, until the best model was achieved. We departed from initial values of 0.20, 0.12, 0.09, and 0.04 km/my for faults A, B, C, and D and ran a set of 65 models, initially varying only fault A and then each of the remaining faults. The best model required velocities of 0.26, 0.18, 0.15, and 0.10 km/my and implied exhumation rates of 0.05 to 0.26 km/my (Figure 13).

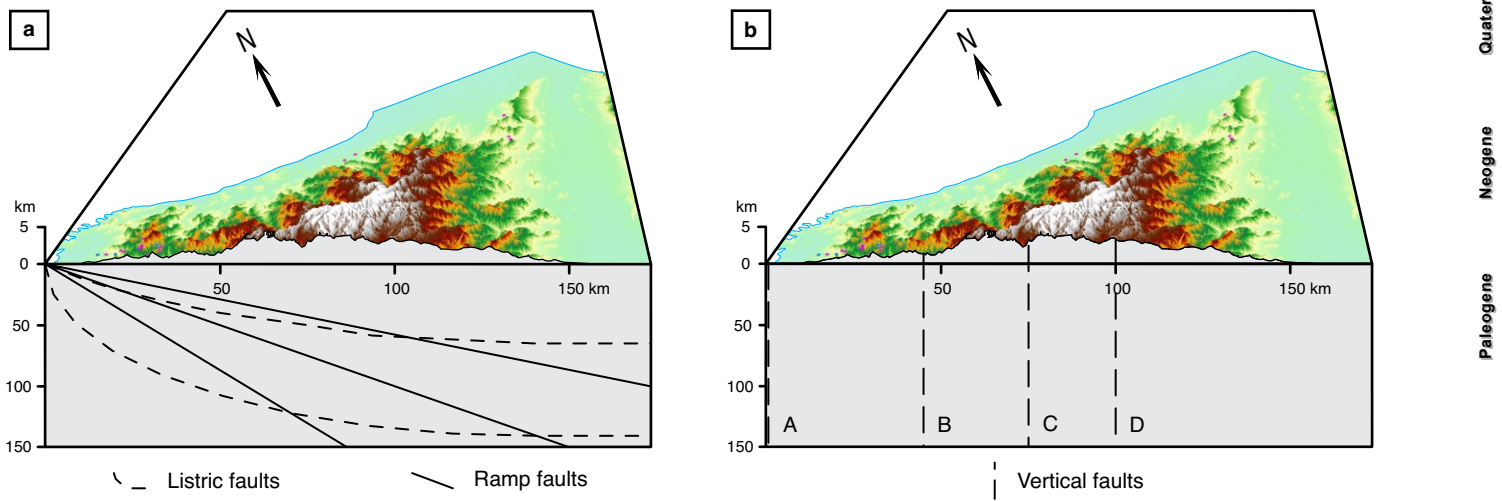


Figure 11. Kinematic scenarios used for Pecube modeling showing the present-day topography and the geometry of faults used for simulations. **(a)** Models of Group 1, showing SE-dipping faults with listric and ramp-only geometries. **(b)** Models of Group 2, showing four vertical faults (A, B, C, D).

Table 4. Typical thermokinematic and elastic parameters used in Pecube.

Parameter (units)	Value
Crustal density (kg/m^3)	2700
Sublithospheric mantle density (kg/m^3)	3200
Equivalent elastic thickness (km)	25
Young modulus (Pa)	1×10^{11}
Poisson's ratio	0.25
Model thickness (km)	40
Thermal diffusivity (km^2/my)	25
Basal model temperature ($^{\circ}\text{C}$)	750
Sea-level temperature ($^{\circ}\text{C}$)	25
Atmospheric lapse rate ($^{\circ}\text{C}/\text{km}$)	6
Crustal heat production ($^{\circ}/\text{my}$)	0
Dpar for AFT calculations (mm)	1.5

5.4.3. Comparison of Model Groups

The best model from each of the two model groups is used for comparison of observed vs. modeled ages along a NW–SE profile (Figure 14a). First, both groups of models reproduce fairly well the pattern of eastward increasing AFT cooling ages as well as the AHe ages (Figure 14b), the latter restricted to the range's NW corner (Figure 14c). We deliberately aimed to obtain plausible exhumation rates coupled to a kinematic model that simulates the observed exhumation gradient rather than attempting to accurately reproduce the range kinematics. However, the modeling results show that a coherent movement

as a single block, as assumed by the SE-dipping fault models (yellow dots in Figure 14), overestimates the AFT ages of the range's eastern end and thus that the compartmentalized model, here approximated with vertical faults, is more likely to represent the actual kinematics (Figure 14d). We note that the spread of observed ages is much larger than that of modeled ages, which we interpret as likely representing observed kinetic variations in particular thermochronometers (chlorine content, grain solubility in AFT, or radiation damage in AHe) that are not captured in this set of models, run with a single kinetic parameter. In summary, we document spatially variable plausible long-term exhumation rates to be lower than 0.25 km/my.

6. Discussion and conclusions

6.1. Episodic Exhumation

We construct a multimethod approach for unravelling exhumation rates in the SNSM by combining 1D calculations derived from bedrock ages and detrital age peaks from multiple thermochronometers, a compilation of age–elevation relationships, and 3D thermokinematic modeling. Together, the combined data unequivocally document episodic exhumation with at least four Cenozoic pulses.

First, triggered by the collision of oceanic terranes along northwestern South America, rapid Paleocene to Eocene (ca. 65–45 Ma) exhumation has been widely recognized in the Central Cordillera (Villagómez & Spikings, 2013) and its northwestern termination at the serranía de San Lucas (Caballero et al., 2013a). A greater magnitude of exhumation farther to the north in the western SNSM precludes the preservation of such

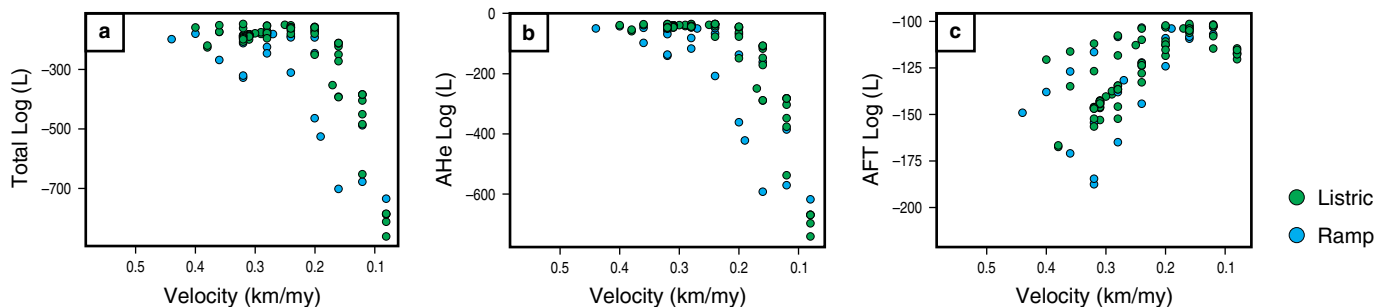


Figure 12. Relation between fault velocity and misfit (evaluated with the log-likelihood, LLH) for ramp and listric fault geometries (Models of Group 1). The highest LLH (i.e., the least negative value) in the upper part of each graph represents the best model. **(a)** Total LLH using both AFT and AHe data. **(b)** LLH using AHe data only. **(c)** LLH using AFT data only.

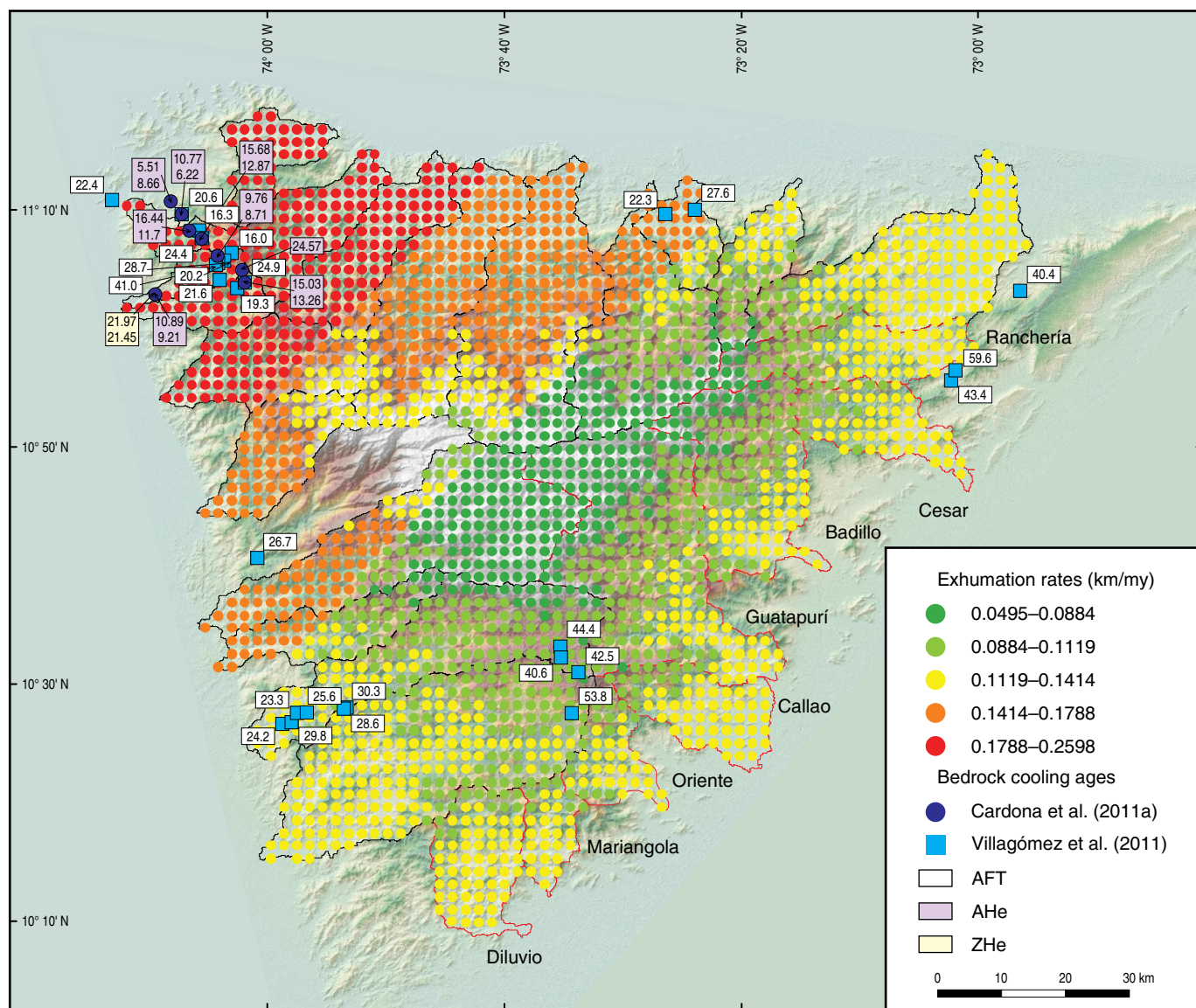


Figure 13. Spatial distributions of exhumation rates for the best solution (i.e., the model with the highest LLH) for Models of Group 2 (vertical faults), showing higher exhumation rates toward the NW.

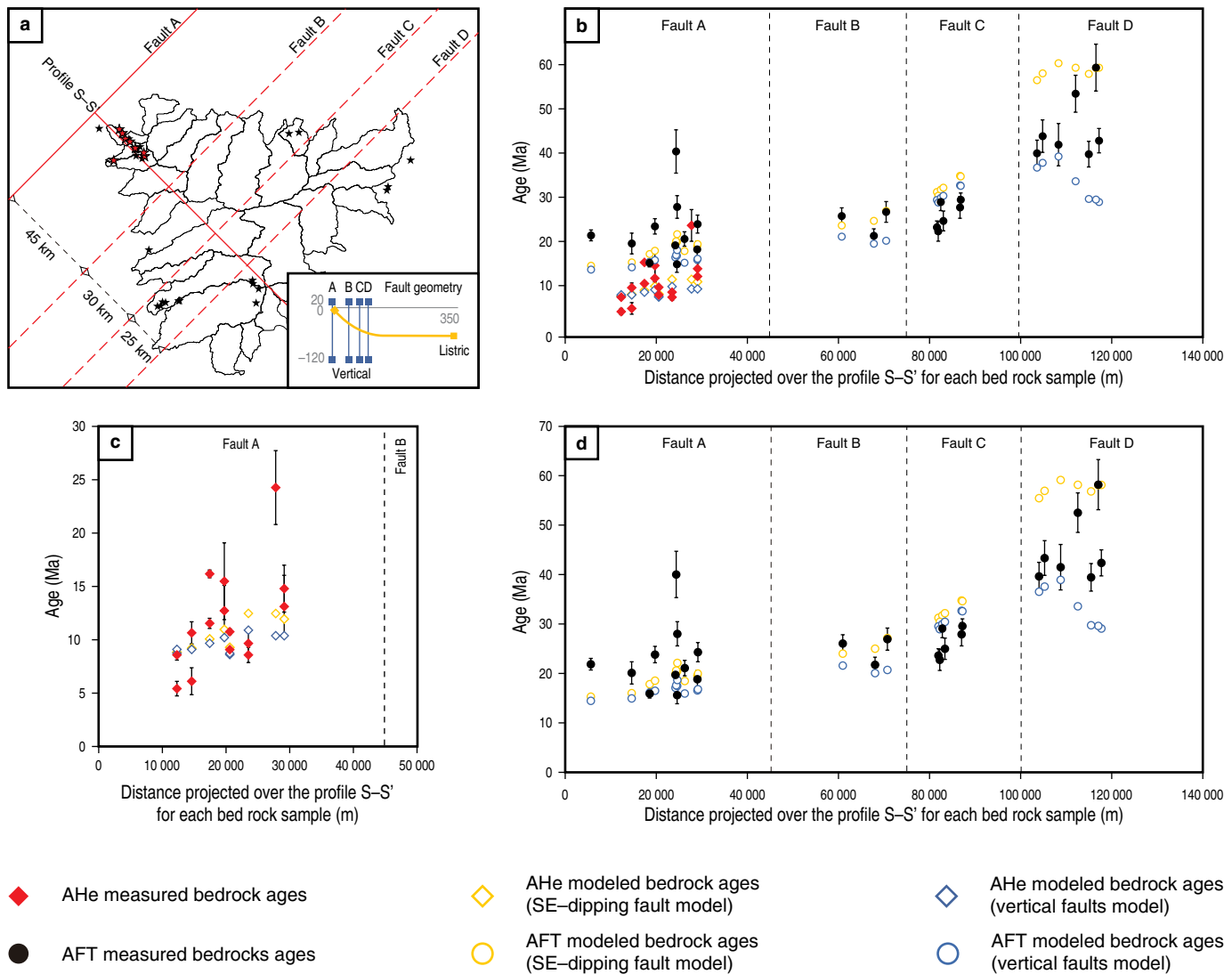


Figure 14. Comparison of the observed ages vs. the modeled ages obtained for the two groups of models, Group 1–SE-dipping faults and Group 2–vertical faults. AHe ages are represented with diamonds and AFT ages with circles; filled symbols are used for observed ages (red for AHe and black for AFT) and hollow symbols are used for modeled ages (yellow for Group 1 and blue for Group 2). **(a)** Distribution of river catchments, locations of faults used for the kinematic simulations, and location of profile S–S' along which ages are projected. Stars are used to represent the sample locations. The inset shows the different geometries used for the two groups of models. **(b)** Comparison of observed vs. modeled AHe and AFT ages for both groups of models. **(c)** Detailed view of observed vs. modeled AHe ages in the northwesternmost 30 km of the profile. **(d)** Observed vs. modeled AFT ages.

a signature; however, it has been recognized in the bedrock (Villagómez et al., 2011) and, recently, in the detrital thermochronological (Patiño, 2018) signature of the eastern SNSM.

A second pulse of moderate to rapid exhumation at 35–20 Ma is evident in (1) age–elevation profiles in the NW and SW sectors of the range (Figure 6), (2) 1D estimates based on available detrital ZFT and AFT ages and assumed closure depths from the western margin (Figure 9, Aracataca), and (3) ubiquitous 30–20 Ma AFT and AHe age peaks across the range.

Third, deceleration of exhumation seems to characterize the post–middle Miocene history of the range, as suggested by

our 1D estimates (Figure 9) and age–elevation profiles (Figure 6). In addition, geobarometry data by Cardona et al. (2011a) suggest that Eocene (56–50 Ma) granitoids cropping out in the range's NW corner were emplaced at pressures between ca. 4.9 and 6.4 kbar, corresponding to depths of 14.7–19.2 km. These estimates imply Eocene to recent exhumation rates of 0.26 to 0.38 km/my in this sector of the range. Our exhumation rates derived from 3D modeling in this area typify lower values, up to 0.26 km/my (Figure 13) for the uppermost ca. 6.5 km of the crust, which is the approximate structural depth sensitive to apatite fission-track data, since the late Oligocene (ca. 25 Ma).

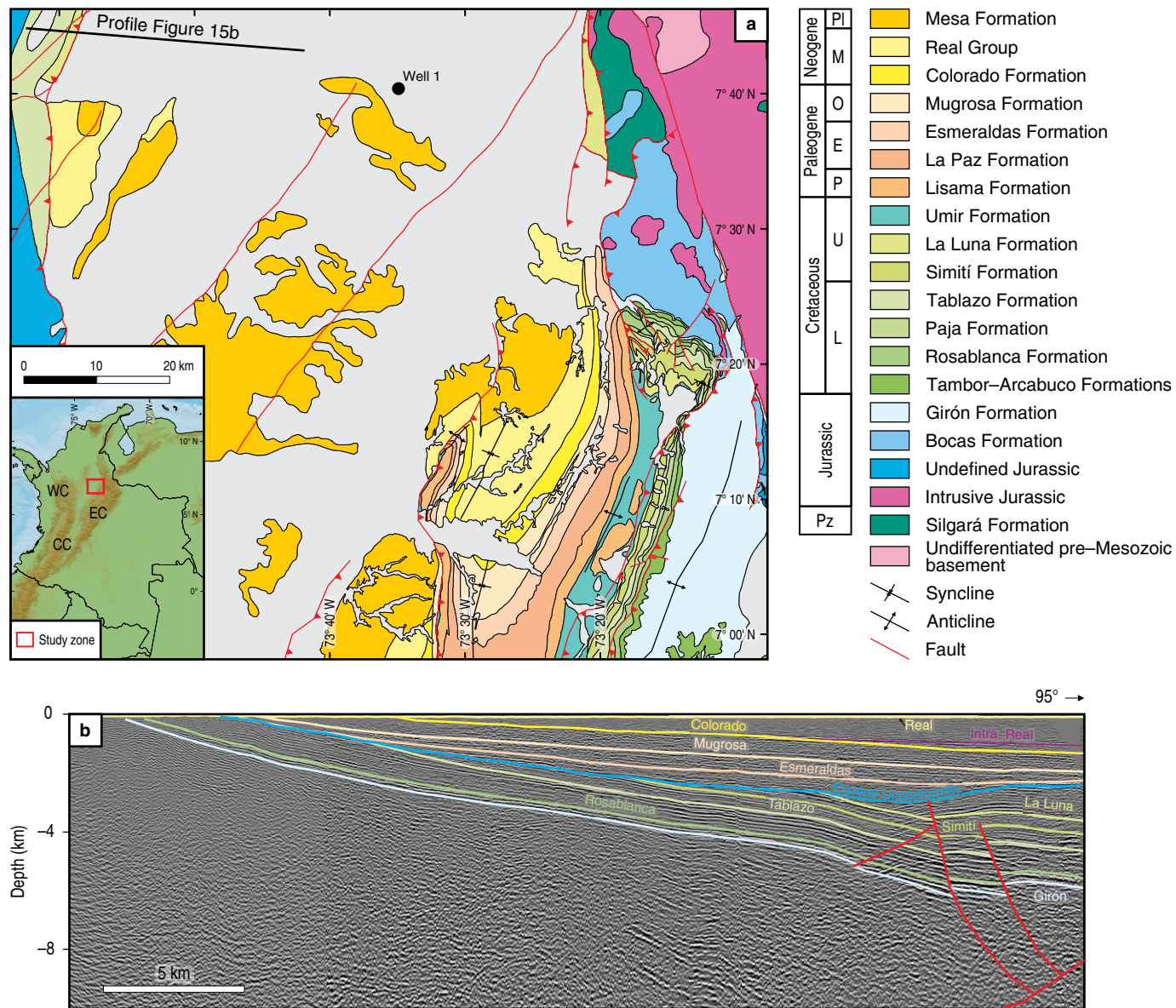


Figure 15. (a) Geologic map of the northern Middle Magdalena Basin and the western foothills of the Eastern Cordillera at ca. 7° N latitude showing the main structures and the location of the seismic line presented in Figure 15b. **(b)** Interpreted seismic line showing onlap of Cenozoic units onto the Central Cordillera’s basement, illustrating progressive southwestward monoclinical tilting of the range. After Parra et al. (2012).

Combined, these independently derived rates suggest that Eocene to late Oligocene rates must have been much faster than post-Oligocene rates.

Finally, both 1D estimations of exhumation rates based on AFT and AHe detrital data from modern sediment (Figure 9) and our 3D modeling results for AFT and AHe data (Figure 13) suggest that the uppermost 2–2.5 km of crust, as documented by AHe data, was exhumed faster than the underlying 2–3 km, as illustrated by AFT data, portraying an acceleration in exhumation at any time since the Miocene. Ongoing work with cosmogenic ¹⁰Be–derived rates in river catchments will help place time constraints on this acceleration.

6.2. Continuity with the Central Cordillera

The structural geometry of the SNSM is that of a southeast-tilted monocline, where extreme exhumation of up to 15–19 km since the Eocene at the NW corner gradually diminishes toward the Cesar–Ranchería Basin, located 100 km to the southeast, where up to 3 km of subsidence occurred in a similar time frame. Such geometry is reminiscent of that of the Central Cordillera, where map patterns (e.g., Gómez et al., 2003) and seismic reflection data (Caballero et al., 2013b; Parra et al., 2012) document progressive onlap of Cenozoic units from the Middle Magdalena Basin onto the Central Cordillera basement (Figure 15a, 15b). As

noted by Gómez et al. (2003), such onlap and the concurrent formation of a westward-expanding pediment surface in the Central Cordillera is the result of the eastward migration of active deformation and related exhumation from the Central to the Eastern Cordillera. Similar structural geometries in the Central Cordillera and the SNSM and basement correlations between both areas across the Sinú–San Jacinto from subsurface data (Montes et al., 2010; Mora–Bohórquez et al., 2017) confirm the hypothesis of former structural continuity of the two ranges.

Exhumation patterns in the Central Cordillera support very rapid initial exhumation in the Late Cretaceous to Paleocene and negligible exhumation (less than 2 km) in the last 40 my (Caballero et al., 2013b; Restrepo–Moreno et al., 2009; Villagómez et al., 2011). Our integrated analyses in Santa Marta also suggest such a decrease in exhumation rates during the initial range development, providing further support for the idea of structural continuity with the Central Cordillera. However, unlike in the latter, where only up to ca. 2 km of exhumation has occurred in the last ca. 40 my, a distinctive pulse of late Eocene – early Miocene rapid exhumation characterizes the entire SNSM and is especially marked at its northwestern corner. We suggest that this pulse beginning at 35 Ma marks the time of tectonic exhumation and dismembering of both ranges through deformation that was accommodated in the form of normal faulting, possibly associated with clockwise rotation (Montes et al., 2010) and the opening of extensional basins in the LMB (Bernal–Olaya et al., 2015; Mora et al., 2018). The oldest known sedimentary fill at 4–5 km depth is Oligocene in age (Montes et al., 2010; Mora et al., 2018; Rincón et al., 2007).

A period of contrasting tectonism and opening of sedimentary basins in the range's northern and western margins followed. Post–Miocene tectonic quiescence led to diminished exhumation rates in the northern slope (Figure 9), which favored sediment retrogradation of the Palomino sequence (Figure 4; Piraquive et al., 2017). In contrast, the western slope continued to be exhumed at faster rates until at least 10 Ma (Figure 9), enhancing the range's structural asymmetry and favoring a reciprocal stratigraphy (Catuneanu et al., 1997), characterized by sediment progradation of the Macaraquilla Conglomerates' Lower Member onto its Upper Member (Figure 3).

Finally, the comparison of AFT and AHe ages presently exposed in the range, retrieved in detrital data from catchments in all three margins, support recent (i.e., post–Miocene) acceleration in exhumation, enhanced in the western margin (Figure 10c). Such a pattern, in the context of steep topography (Figure 1a, 1c) and a humid climate (Figure 1d), supports the concept of a very recent exhumation pulse in line with the hypothesis of denudational immaturity, whereby recent crustal stacking and rock uplift would exceed the magnitude of exhumation, generating a non–steady–state (i.e., rising) topography. Diminished

crustal thickness in the range's NW corner (25–35 km, Figure 1b) and a positive gravity anomaly (Figure 1a) allow us to postulate a likely removal of the lower crust as the trigger of such a recent episode. Ongoing work on recent denudation rates with cosmogenic radionuclides will help place more detailed time constraints on this rapid recent exhumation.

Acknowledgments

This research was funded by the São Paulo Research Foundation (FAPESP) Youth Researcher Grant 2013/03265–5 to Mauricio PARRA. The contributions by Sebastián ECHEVERRI and Ana María PATIÑO constitute part of their PhD and MS theses, respectively, at the Universidade de São Paulo, funded by the CAPES Foundation. Juan Carlos RAMÍREZ acknowledges the funding provided by the FAPESP Grant 2016/10094–0 for his PhD thesis, part of which is included in this work. We thank Frederico GENEZINI from IPEN–USP for diligently facilitating neutron irradiation for fission–track dating. Alexandre ALVES and Ana Beatriz de BARROS at IEE–USP and Thays MINELLI at IGC–USP graciously assisted with thermochronology sample preparation. We appreciate the kind collaboration of the TODARO family (Aracataca) and Juan Carlos and Florencia (Palomino) during fieldwork.

References

- Agencia Nacional de Hidrocarburos. 2010. Mapa de Anomalía de Bouguer Total de la República de Colombia. Scale 1: 2 500 000. Bogotá. https://www.anh.gov.co/Informacion-Geologica-y-Geofisica/Pais/Documents/ANOMALIA_DE_BOUGUER_TOTAL_DE_LA_REPUBLICA_DE_COLOMBIA%202010.pdf (consulted in June 2017).
- Allen, P.A. & Allen, J.R. 2005. Basin Analysis: Principles and Applications. Blackwell Publishing company, 549 p. Oxford.
- Ayala, R.C., Bayona, G., Ojeda, C., Cardona, A., Valencia, V., Padron, C., Yoris, F., Mesa, J. & Garcia, A. 2009. Estratigrafía y procedencia de las unidades comprendidas entre el Campaniano y el Paleógeno en la Subcuenca de Cesar: Aportes a la evolución tectónica del área. *Geología Colombiana*, (34): 3–33.
- Ayala, R.C., Bayona, G., Cardona, A., Ojeda, C., Montenegro, O.C., Montes, C., Valencia, V. & Jaramillo, C. 2012. The Paleogene synorogenic succession in the northwestern Maracaibo Block: Tracking intraplate uplifts and changes in sediment delivery systems. *Journal of South American Earth Sciences*, 39: 93–111. <https://doi.org/10.1016/j.jsames.2012.04.005>
- Bayona, G., Lamus–Ochoa, F., Cardona, A., Jaramillo, C., Montes, C. & Tchegliakova, N. 2007. Procesos orogénicos del Paleógeno para la Cuenca de Ranchería (Guajira, Colombia) y áreas adyacentes definidos por análisis de procedencia. *Geología Colombiana*, (32): 21–46.

- Bayona, G., Jiménez, G., Silva, C., Cardona, A., Montes, C., Roncancio, J. & Cordani, U. 2010. Paleomagnetic data and K–Ar ages from Mesozoic units of the Santa Marta Massif: A preliminary interpretation for block rotation and translations. *Journal of South American Earth Sciences*, 29(4): 817–831. <https://doi.org/10.1016/j.jsames.2009.10.005>
- Bayona, G., Cardona, A., Jaramillo, C., Mora, A., Montes, C., Valencia, V., Ayala, C., Montenegro, O. & Ibañez–Mejía, M. 2012. Early Paleogene magmatism in the northern Andes: Insights on the effects of oceanic plateau–continent convergence. *Earth and Planetary Science Letters*, 331–332: 97–111. <https://doi.org/10.1016/j.epsl.2012.03.015>
- Bernal–Olaya, R., Mann, P. & Escalona, A. 2015. Cenozoic tectonostratigraphic evolution of the Lower Magdalena Basin, Colombia: An Example of an under–to overfilled forearc basin. In: Bartolini, C. & Mann, P. (editors), *Petroleum geology and potential of the Colombian Caribbean margin*. American Association of Petroleum Geologists, Memoir 108, p. 345–398. <https://doi.org/10.1306/13531943M1083645>
- Braun, J. 2002. Quantifying the effect of recent relief changes on age–elevation relationships. *Earth and Planetary Science Letters*, 200(3–4): 331–343. [https://doi.org/10.1016/S0012-821X\(02\)00638-6](https://doi.org/10.1016/S0012-821X(02)00638-6)
- Braun, J. 2003. Pecube: A new finite–element code to solve the 3D heat transport equation including the effects of a time–varying, finite amplitude surface topography. *Computers & Geosciences*, 29(6): 787–794. [https://doi.org/10.1016/S0098-3004\(03\)00052-9](https://doi.org/10.1016/S0098-3004(03)00052-9)
- Braun, J., van der Beek, P., Valla, P., Robert, X., Herman, F., Glotzbach, C., Pedersen, V., Perry, C., Simon–Labric, T. & Prigent, C. 2012. Quantifying rates of landscape evolution and tectonic processes by thermochronology and numerical modeling of crustal heat transport using PECUBE. *Tectonophysics*, 524–525: 1–28. <https://doi.org/10.1016/j.tecto.2011.12.035>
- Burke, K., Cooper, C., Dewey, J.F., Mann, P. & Pindell, J.L. 1984. Caribbean tectonics and relative plate motions. In: Bonini, W.E., Hargraves, R.B. & Shagam, R. (editors), *The Caribbean–South American plate boundary and regional tectonics*. Geological Society of America, Memoir 162, p. 31–63. <https://doi.org/10.1130/MEM162-p31>
- Caballero, V., Parra, M., Mora, A., López, C., Rojas, L.E. & Quintero, I. 2013a. Factors controlling selective abandonment and reactivation in thick–skin orogens: A case study in the Magdalena Valley, Colombia. In: Nemčok, M., Mora, A. & Cosgrove, J.W. (editors), *Thick–skin–dominated orogens: From initial inversion to full accretion*. Geological Society of London, Special Publication 377, p. 343–367. London. <https://doi.org/10.1144/SP377.4>
- Caballero, V., Mora, A., Quintero, I., Blanco, V., Parra, M., Rojas, L.E., López, C., Sánchez, N., Horton, B.K., Stockli, D. & Duddy, I. 2013b. Tectonic controls on sedimentation in an intermontane hinterland basin adjacent to inversion structures: The Nuevo Mundo Syncline, Middle Magdalena Valley, Colombia. In: Nemčok, M., Mora, A. & Cosgrove, J.W. (editors), *Thick–skin–dominated orogens: From initial inversion to full accretion*. Geological Society of London, Special Publication 377, p. 315–342. London. <https://doi.org/10.1144/SP377.12>
- Cadena, A.F., & Slatt, R.M. 2013. Seismic and sequence stratigraphic interpretation of the area of influence of the Magdalena submarine fan, offshore northern Colombia. *Interpretation*, 1(1): SA53–SA74. <https://doi.org/10.1190/INT-2013-0028.1>
- Cardona, A., Cordani, U.G. & MacDonald, W.D. 2006. Tectonic correlations of pre–Mesozoic crust from the northern termination of the Colombian Andes, Caribbean region. *Journal of South American Earth Sciences*, 21(4): 337–354. <https://doi.org/10.1016/j.jsames.2006.07.009>
- Cardona, A., Chew, D., Valencia, V.A., Bayona, G., Miškovčić, A. & Ibañez–Mejía, M. 2010a. Grenvillian remnants in the northern Andes: Rodinian and Phanerozoic paleogeographic perspectives. *Journal of South American Earth Sciences*, 29(1): 92–104. <https://doi.org/10.1016/j.jsames.2009.07.011>
- Cardona, A., Valencia, V., Garzón, A., Montes, C., Ojeda, G., Ruiz, J. & Weber, M. 2010b. Permian to Triassic I to S–type magmatic switch in the northeast Sierra Nevada de Santa Marta and adjacent regions, Colombian Caribbean: Tectonic setting and implications within Pangea paleogeography. *Journal of South American Earth Sciences*, 29(4): 772–783. <https://doi.org/10.1016/j.jsames.2009.12.005>
- Cardona, A., Valencia, V., Bustamante, C., García–Casco, A., Ojeda, G., Ruiz, J., Saldarriaga, M. & Weber, M. 2010c. Tectonomagmatic setting and provenance of the Santa Marta Schists, northern Colombia: Insights on the growth and approach of Cretaceous Caribbean oceanic terranes to the South American continent. *Journal of South American Earth Sciences*, 29(4): 784–804. <https://doi.org/10.1016/j.jsames.2009.08.012>
- Cardona, A., Valencia, V., Weber, M., Duque, J., Montes, C., Ojeda, G.Y., Reiners, P., Domanik, K., Nicolescu, S. & Villagómez, D. 2011a. Transient Cenozoic tectonic stages in the southern margin of the Caribbean plate: U–Th/He thermochronological constraints from Eocene plutonic rocks in the Santa Marta Massif and serranía de Jararará, northern Colombia. *Geologica Acta*, 9(3): 445–466. <https://doi.org/10.1344/105.000001739>
- Cardona, A., Valencia, V., Bayona, G., Duque, J., Ducea, M., Gehrels, G., Jaramillo, C., Montes, C., Ojeda, G. & Ruiz, J. 2011b. Early–subduction–related orogeny in the northern Andes: Turonian to Eocene magmatic and provenance record in the Santa Marta Massif and Ranchería Basin, northern Colombia. *Terra Nova*, 23(1): 26–34. <https://doi.org/10.1111/j.1365-3121.2010.00979.x>
- Case, J.E., & MacDonald, W.D. 1973. Regional gravity anomalies and crustal structure in northern Colombia. *Geological Society of America Bulletin*, 84(9): 2905–2916. [https://doi.org/10.1130/0016-7606\(1973\)84<2905:RGAACS>2.0.CO;2](https://doi.org/10.1130/0016-7606(1973)84<2905:RGAACS>2.0.CO;2)
- Catuneanu, O., Beaumont, C. & Waschbusch, P. 1997. Interplay of static loads and subduction dynamics in foreland basins: Re-

- reciprocal stratigraphies and the “missing” peripheral bulge. *Geology*, 25(12): 1087–1090. [https://doi.org/10.1130/0091-7613\(1997\)025<1087:IOSLAS>2.3.CO;2](https://doi.org/10.1130/0091-7613(1997)025<1087:IOSLAS>2.3.CO;2)
- Cediel, F., Shaw, R.P. & Cáceres, C. 2003. Tectonic assembly of the northern Andean Block. In: Bartolini, C., Buffler, R.T. & Blickwede, J. (editors), *The circum-Gulf of Mexico and the Caribbean: Hydrocarbon habitats, basin formation, and plate tectonics*. American Association of Petroleum Geologists, Memoir 79, p. 815–848. Tulsa, USA.
- Ceron, J.F. 2008. Crustal structure of the Colombian Caribbean Basin and margins. Doctoral thesis, University of South Carolina, 181 p. Columbia.
- Ceron, J.F., Kellogg, J.N. & Ojeda, G.Y. 2007. Basement configuration of the northwestern South America–Caribbean margin from recent geophysical data. *Ciencia, Tecnología y Futuro*, 3(3): 25–49.
- Colmenares, F.H., Mesa, A.M., Roncancio, J.H., Arciniegas, E.G., Pedraza, P.E., Cardona, A., Romero, A.J., Silva, C.A., Alvarado, S.I., Romero, O.A. & Vargas, A.F. 2007. Geología de las planchas 11, 12, 13, 14, 18, 19, 20, 21, 25, 26, 27, 33, 34 y 40. Proyecto: Evolución geohistórica de la Sierra Nevada de Santa Marta. Invenmar–Ingeominas–ICP–Ecopetrol–Geosearch Ltda., 401 p. Bogotá.
- Cordani, U.G., Cardona, A., Jiménez, D.M., Liu, D. & Nutman, A.P. 2005. Geochronology of Proterozoic basement inliers in the Colombian Andes: Tectonic history of remnants of a fragmented Grenville belt. In: Vaughan, A.P.M., Leat, P.T. & Pankhurst, R.J. (editors), *Terrane processes at the margins of Gondwana*. Geological Society of London, Special Publication 246, p. 329–346. London. <https://doi.org/10.1144/GSL.SP.2005.246.01.13>
- Dodson, M.H. 1973. Closure temperature in cooling geochronological and petrological systems. *Contributions to Mineralogy and Petrology*, 40(3): 259–274. <https://doi.org/10.1007/BF00373790>
- Donelick, R.A., O’Sullivan, P.B. & Ketcham, R.A. 2005. Apatite fission-track analysis. *Reviews in Mineralogy and Geochemistry*, 58(1): 49–94. <https://doi.org/10.2138/rmg.2005.58.3>
- Duque–Caro, H. 1984. Structural style, diapirism, and accretionary episodes of the Sinú–San Jacinto terrane, southwestern Caribbean bordeland. In: Bonini, W.E., Hargraves, R.B. & Shagam, R. (editors), *The Caribbean–South American plate boundary and regional tectonics*. Geological Society of America, Memoir 162, p. 303–316. <https://doi.org/10.1130/MEM162-p303>
- Duque, J.F. 2010. Geocronología (U/Pb y $^{40}\text{Ar}/^{39}\text{Ar}$) y geoquímica de los intrusivos paleógenos de la Sierra Nevada de Santa Marta y sus relaciones con la tectónica del Caribe y el arco magmático circum-caribeño. Master thesis, Universidad Nacional Autónoma de México, 189 p. México D. F.
- Echeverri, S. 2019. Cenozoic tectonic evolution of the Sierra Nevada of Santa Marta, northern Colombia: A record of strike–slip tectonics along the southern Caribbean Plate. Doctoral Thesis, Universidade de São Paulo, 350 p. Brasil.
- Echeverri, S., Parra, M., Sobel, E., Pardo, A., Trejos, R., Vallejo, F. & Patiño, A.M. 2017. Registro de exhumación cenozoica de la Sierra Nevada de Santa Marta, Colombia: Entendiendo la interacción entre tectónica y sedimentación a partir de datos de proveniencia y termocronología de baja temperatura. XVI Congreso Colombiano de Geología. *Memoirs*, p. 1495–1500. Santa Marta.
- Farley, K.A. 2002. (U–Th)/He Dating: Techniques, calibrations, and applications. *Reviews in Mineralogy and Geochemistry*, 47(1): 819–844. <https://doi.org/10.2138/rmg.2002.47.18>
- Flowers, R.M., Ketcham, R.A., Shuster, D.L. & Farley, K.A. 2009. Apatite (U–Th)/He thermochronometry using a radiation damage accumulation and annealing model. *Geochimica et Cosmochimica Acta*, 73(8): 2347–2365. <https://doi.org/10.1016/j.gca.2009.01.015>
- Galbraith, R.F. 1981. On statistical models for fission track counts. *Journal of the International Association for Mathematical Geology*, 13(6): 471–478
- Gallagher, K., Brown, R. & Johnson, C. 1998. Fission track analysis and its applications to geological problems. *Annual Review of Earth and Planetary Sciences*, 26(1): 519–572. <https://doi.org/10.1146/annurev.earth.26.1.519>
- Gautheron, C., Tassan-Got, L., Barbarand, J. & Pagel, M. 2009. Effect of alpha–damage annealing on apatite (U–Th)/He thermochronology. *Chemical Geology*, 266(3–4): 157–170. <https://doi.org/10.1016/j.chemgeo.2009.06.001>
- Gómez, E., Jordan, T., Allmendinger, R., Hegarty, K., Kelley, S. & Heizler, M. 2003. Controls on architecture of the Late Cretaceous to Cenozoic southern Middle Magdalena Valley Basin, Colombia. *Geological Society of America Bulletin*, 115(2): 131–147. [https://doi.org/10.1130/0016-7606\(2003\)115<0131:COAOTL>2.0.CO;2](https://doi.org/10.1130/0016-7606(2003)115<0131:COAOTL>2.0.CO;2)
- Gorney, D., Escalona, A., Mann, P., Magnani, M.B., Levander, A., Christeson, G., Mann, P., Zelt, C.A., Magnani, M.B., Schmitz, M., Clark, S., Guedez, M.C., Bezada, M., Arogunmati, Y., Gorney, D., Aitken, T. & Beardsley, A. 2007. Chronology of Cenozoic tectonic events in western Venezuela and the Leeward Antilles based on integration of offshore seismic reflection data and on–land geology. *American Association of Petroleum Geology Bulletin*, 91(5): 653–684. <https://doi.org/10.1306/11280606002>
- Green, P.F. 1981. A new look at statistics in fission–track dating. *Nuclear Tracks*, 5(1–2): 77–86. [https://doi.org/10.1016/0191-278X\(81\)90029-9](https://doi.org/10.1016/0191-278X(81)90029-9)
- Harrison, T.M. & Zeitler, P.K. 2005. Fundamentals of noble gas thermochronology. In: Reiners, P.W. & Ehlers, T.A. (editors), *Low temperature thermochronology: Techniques, interpretations, and applications*. Mineralogical Society of America, *Reviews in Mineralogy and Geochemistry* 58, p. 123–149. Washington D.C.
- Hernández, M., Maldonado, I., González, J., Martínez, H., Clavijo, J. & Reyes, G. 2003. Memoria explicativa: Geología de las

- planchas 25 Fundación, 32 Monterrubio y 39 El Difícil. Scale 1:100 000. Ingeominas, 74 p. Bogotá.
- Idárraga–García, J. & Romero, J. 2010. Neotectonic study of the Santa Marta Fault System, western foothills of the Sierra Nevada de Santa Marta, Colombia. *Journal of South American Earth Sciences*, 29(4): 849–860. <https://doi.org/10.1016/j.jsames.2009.11.004>
- Jaramillo, C., Rueda, M. & Torres, V. 2011. A palynological zonation for the Cenozoic of the Llanos and Llanos Foothills of Colombia. *Palynology*, 35(1): 46–84. <https://doi.org/10.1080/01916122.2010.515069>
- Kellogg, J.N. 1984. Cenozoic tectonic history of the sierra de Perijá, Venezuela–Colombia, and adjacent basins. In: Bonini, W.E., Hargraves, R.B. & Shagam, R. (editors), *The Caribbean–South American Plate boundary and regional tectonics*. Geological Society of America, Memoir 162, p. 239–261. <https://doi.org/10.1130/MEM162-p239>
- Kellogg, J.N. & Bonini, W.E. 1982. Subduction of the Caribbean Plate and basement uplifts in the overriding South American Plate. *Tectonics*, 1(3): 251–276. <https://doi.org/10.1130/MEM162-p239>
- Mann, P., Escalona, A. & Castillo, M.V. 2006. Regional geologic and tectonic setting of the Maracaibo supergiant Basin, western Venezuela. *American Association of Petroleum Geologists Bulletin*, 90(4): 445–477. <https://doi.org/10.1306/10110505031>
- McMahon, C. 2000. Evaluation of the effects of oblique collision between the Caribbean and South American Plates using geochemistry from igneous and metamorphic bodies of northern Venezuela. Doctoral Thesis, University of Notre Dame, 277 p. Paris.
- Montes, C., Guzmán, G., Bayona, G., Cardona, A., Valencia, V. & Jaramillo, C. 2010. Clockwise rotation of the Santa Marta Massif and simultaneous Paleogene to Neogene deformation of the Plato–San Jorge and Cesar–Ranchería Basins. *Journal of South American Earth Sciences*, 29(4): 832–848. <https://doi.org/10.1016/j.jsames.2009.07.010>
- Montes, C., Cardona, A., Jaramillo, C., Pardo, A., Silva, J.C., Valencia, V., Ayala, C., Pérez–Ángel, L.C., Rodríguez–Parra, L.A., Ramírez, V. & Niño, H. 2015. Middle Miocene closure of the Central American Seaway. *Science*, 348(6231): 226–229. <https://doi.org/10.1126/science.aaa2815>
- Mora–Bohórquez, J.A., Ibañez–Mejía, M., Oncken, O., de Freitas, M., Vélez, V., Mesa, A. & Serna, L. 2017. Structure and age of the Lower Magdalena Valley Basin basement, northern Colombia: New reflection–seismic and U–Pb–Hf insights into the termination of the central Andes against the Caribbean Basin. *Journal of South American Earth Sciences*, 74: 1–26. <https://doi.org/10.1016/j.jsames.2017.01.001>
- Mora, J.A., Oncken, O., Le Breton, E., Mora, A., Veloza, G., Vélez, V. & de Freitas, M. 2018. Controls on forearc basin formation and evolution: Insights from Oligocene to recent tectono–stratigraphy of the Lower Magdalena Valley basin of northwest Colombia. *Marine and Petroleum Geology*, 97: 288–310. [https://doi.org/10.1016/S0895-9811\(02\)00017-2](https://doi.org/10.1016/S0895-9811(02)00017-2)
- Mulligan, M. 2006. Global gridded 1km TRMM rainfall climatology and derivatives, version 1.0 Database: <http://www.ambiotek.com/1kmrainfall> (consulted in November 2017).
- Ordóñez–Carmona, O. & Pimentel, M.M. 2002. Rb–Sr and Sm–Nd isotopic study of the Puquí Complex, Colombian Andes. *Journal of South American Earth Sciences*, 15(2): 173–182. [https://doi.org/10.1016/S0895-9811\(02\)00017-2](https://doi.org/10.1016/S0895-9811(02)00017-2)
- Parra, M., Mora, A., López, C., Rojas, L.E. & Horton, B.K. 2012. Detecting earliest shortening and deformation advance in thrust belt hinterlands: Example from the Colombian Andes. *Geology*, 40(2): 175–178. <https://doi.org/10.1130/G32519.1>
- Parra, M., Echeverri, J.S., Perez–Consuegra, N. & Senatore, C.A. 2016. Episodic uplift patterns of the Sierra Nevada de Santa Marta in northern Colombia. 10th South American Symposium on Isotope Geology. Program and Abstracts, 1, p. 72. Puerto Vallarta, México.
- Patiño, A.M. 2018. Cenozoic exhumation patterns in the eastern Sierra Nevada de Santa Marta, northern Colombia: A detrital thermochronometry study. Master thesis, Universidade de São Paulo, 115 p. São Paulo. <https://doi.org/10.11606/D.44.2018.tde-17072018-144314>
- Pindell, J.L., Higgs, R. & Dewey, J.F. 1998. Cenozoic palinspastic reconstruction, paleogeographic evolution and hydrocarbon setting of the northern margin of South America. In: Pindell, J.L. & Drake, C. (editors), *Paleogeographic evolution and non–glacial eustasy, northern South America*. Society for Sedimentary Geology, Special Publication 58, p. 45–85. <https://doi.org/10.2110/pec.98.58.0045>
- Pindell, J.L. & Kennan, L. 2009. Tectonic evolution of the Gulf of Mexico, Caribbean and northern South America in the mantle reference frame: An update. In: James, K.H., Lorente, M.A. & Pindell, J.L. (editors), *The origin and evolution of the Caribbean Plate*. Geological Society of London, Special Publication 328, p. 1–55. <https://doi.org/10.1144/SP328.1>
- Pinzón–Rodríguez, E.M. 2014. Caracterización litológica y sedimentológica de una unidad conglomerática en cercanías de Aracataca y su significado para el levantamiento de la Sierra Nevada de Santa Marta (SNSM). Bachelor thesis, Universidad Nacional de Colombia, 21 p. Bogotá.
- Piraquive, A., Pinzón, E., Kammer, A., Bernet, M. & von Quadt, A. 2017. Early Neogene unroofing of the Sierra Nevada de Santa Marta, as determined from detrital geothermochronology and the petrology of clastic basin sediments. *Geological Society of America Bulletin*, 130(3–4): 355–380. <https://doi.org/10.1130/B31676.1>
- Reiners, P.W., & Brandon, M.T. 2006. Using thermochronology to understand orogenic erosion. *Annual Review Earth Plane-*

- tary Sciences, 34: 419–466. <https://doi.org/10.1146/annurev.earth.34.031405.125202>
- Restrepo–Moreno, S.A., Foster, D.A., Stockli, D.F. & Parra–Sánchez, L.N. 2009. Long–term erosion and exhumation of the “Altiplano Antioqueño,” northern Andes (Colombia) from apatite (U–Th)/He thermochronology. *Earth and Planetary Science Letters*, 278(1–2): 1–12. <https://doi.org/10.1016/j.epsl.2008.09.037>
- Restrepo–Pace, P.A., Ruiz, J., Gehrels, G. & Cosca, M. 1997. Geochronology and Nd isotopic data of Grenville–age rocks in the Colombian Andes: New constraints for late Proterozoic – early Paleozoic paleocontinental reconstructions of the Americas. *Earth and Planetary Science Letters*, 150(3–4): 427–441. [https://doi.org/10.1016/S0012-821X\(97\)00091-5](https://doi.org/10.1016/S0012-821X(97)00091-5)
- Restrepo, J.J., Ordóñez–Carmona, O., Armstrong, R. & Pimentel, M.M. 2011. Triassic metamorphism in the northern part of the Tahamí Terrane of the Central Cordillera of Colombia. *Journal of South American Earth Sciences*, 32(4): 497–507. <https://doi.org/10.1016/j.jsames.2011.04.009>
- Reyes, H.A., Montenegro, B.M. & Gómez, P.D. 2004. Tectonoestratigrafía y evolución del Valle Inferior del Magdalena. *Boletín de Geología*, 26(42): 19–38.
- Rincón, D.A., Arenas, J.E., Cuartas, C.H., Cárdenas, A.L., Molineros, C.E., Caicedo, C. & Jaramillo, C. 2007. Eocene–Pliocene planktonic foraminifera biostratigraphy from the continental margin of the southwest Caribbean. *Stratigraphy*, 4(4): 261–311.
- Ruiz, G.M.H., Seward, D. & Winkler, W. 2004. Detrital thermochronology – a new perspective on hinterland tectonics, an example from the Andean Amazon Basin, Ecuador. *Basin Research*, 16(3): 413–430. <https://doi.org/10.1111/j.1365-2117.2004.00239.x>
- Salazar, C.A., Bustamante, C. & Archanjo, C.J. 2016. Magnetic fabric (AMS, AAR) of the Santa Marta Batholith (northern Colombia) and the shear deformation along the Caribbean Plate margin. *Journal of South American Earth Sciences*, 70: 55–68. <https://doi.org/10.1016/j.jsames.2016.04.011>
- Sánchez, J. & Mann, P. 2015. Integrated structural and basinal analysis of the Cesar–Ranchería Basin, Colombia: Implications for its tectonic history and petroleum systems. In: Bartolini, C. & Mann, P. (editors), *Petroleum geology and potential of the Colombian Caribbean Margin*. American Association of Petroleum Geologists, *Memoirs* 108, p. 431–470. <https://doi.org/10.1306/13531945M1083648>
- Tagami, T. & O’Sullivan, P.B. 2005. Fundamentals of fission–track thermochronology. In: Reiners, P.W. & Ehlers, T.A. (editors), *Low temperature thermochronology: Techniques, interpretations, and applications*. Mineralogical Society of America, *Reviews in Mineralogy and Geochemistry* 58, p. 19–47. Washington.
- Trenkamp, R., Kellogg, J.N., Freymueller, J.T. & Mora, H. 2002. Wide plate margin deformation, southern Central America and northwestern South America, CASA GPS observations. *Journal of South American Earth Sciences*, 15(2): 157–171. [https://doi.org/10.1016/S0895-9811\(02\)00018-4](https://doi.org/10.1016/S0895-9811(02)00018-4)
- Tschanz, C.M., Jimeno, A. & Cruz, J. 1969. *Geology of the Sierra Nevada de Santa Marta area (Colombia): Preliminary report*. Ingeominas, 288 p. Bogotá.
- Tschanz, C.M., Marvin, R.F., Cruz, J., Mehnert, H.H. & Cebula, G.T. 1974. Geologic evolution of the Sierra Nevada de Santa Marta, northeastern Colombia. *Geological Society of America Bulletin*, 85(2): 273–284. [https://doi.org/10.1130/0016-7606\(1974\)85<273:GEOTSN>2.0.CO;2](https://doi.org/10.1130/0016-7606(1974)85<273:GEOTSN>2.0.CO;2)
- Vermeesch, P. 2012. On the visualization of detrital age distributions. *Chemical Geology*, 312–313: 190–194. <https://doi.org/10.1016/j.chemgeo.2012.04.021>
- Villagómez, D. & Spikings, R. 2013. Thermochronology and tectonics of the Central and Western Cordilleras of Colombia: Early Cretaceous – Tertiary evolution of the northern Andes. *Lithos*, 160–161: 228–249. <https://doi.org/10.1016/j.lithos.2012.12.008>
- Villagómez, D., Spikings, R., Mora, A., Guzmán, G., Ojeda, G., Cortés, E. & van der Lelij, R. 2011. Vertical tectonics at a continental crust–oceanic plateau plate boundary zone: Fission track thermochronology of the Sierra Nevada de Santa Marta, Colombia. *Tectonics*, 30(4): 1–18. <https://doi.org/10.1029/2010TC002835>
- Vinasco, C.J., Cordani, U.G., González, H., Weber, M. & Peláez, C. 2006. Geochronological, isotopic, and geochemical data from Permo – Triassic granitic gneisses and granitoids of the Colombian central Andes. *Journal of South American Earth Sciences*, 21(4): 355–371. <https://doi.org/10.1016/j.jsames.2006.07.007>
- Weber, M., Cardona, A., Paniagua, F., Cordani, U., Sepúlveda, L. & Wilson, R. 2009. The Cabo de la Vela mafic–ultramafic complex, northeastern Colombian Caribbean region: A record of multistage evolution of a Late Cretaceous intra–oceanic arc. In: James, K.H., Lorente, M.A. & Pindell, J.L. (editors), *The origin and evolution of the Caribbean Plate*. Geological Society of London, *Special Publication* 328, p. 549–568. <https://doi.org/10.1144/SP328.22>
- Yarce, J., Monsalve, G., Becker, T.W., Cardona, A., Poveda, E., Alvira, D. & Ordóñez–Carmona, O. 2014. Seismological observations in northwestern South America: Evidence for two subduction segments, contrasting crustal thicknesses and upper mantle flow. *Tectonophysics*, 637: 57–67. <https://doi.org/10.1016/j.tecto.2014.09.006>

Explanation of Acronyms, Abbreviations, and Symbols:

AFT	Apatite fission-track	ND	Number of induced tracks counted in the mica for estimating Rho-D
AHe	(U-Th)/He in apatites	NI	Number of induced tracks counted for estimating Rho-I
CAPES	Coordination for the Improvement of Higher Education Personnel	NS	Number of spontaneous tracks counted for estimating Rho-S
ESR	Equivalent-sphere radius	Rho-D	Induced track density
eU	Effective uranium content	Rho-I	Induced tracks density measured
IEE-USP	Institute of Energy and Environment, Universidade de São Paulo	Rho-S	Spontaneous tracks density measured
IGc-USP	Institute of Geosciences, Universidade de São Paulo	SNSM	Sierra Nevada de Santa Marta
IPEN-USP	Institute of Energy and Nuclear Research, Universidade de São Paulo	SRTM 90	Shuttle Radar Topography Mission – Resolution 90 meters
LLH	Log-likelihood function	TRMM	Tropical Rainfall Measuring Mission
LMB	Lower Magdalena Basin	ZFT	Zircon fission-track
		ZHe	(U-Th)/He in zircons

Authors' Biographical Notes



Mauricio PARRA is an Assistant Professor at the Instituto de Energia e Ambiente of the Universidade de São Paulo, where he leads the Low-Termochronology Laboratory. He received his BS in geology from the Universidad Nacional de Colombia and his PhD from the Institut für Geowissenschaften, Universität Potsdam. His research focuses on the tectonic evolution of mountain belts

using thermochronometry and sedimentary basin analysis.



Ana María PATIÑO is graduated from the Universidad Nacional de Colombia Sede Medellín. She received a master's degree in Earth sciences at the Universidade de São Paulo, Brasil. She has worked with regional geology issues employing techniques such as geochronology and low-temperature thermochronology. Her research interests include tectonic geology, orogenetic processes, and landscape evolution.



Sebastián ECHEVERRI is a geologist from the Universidad de Caldas, with an MS in Earth sciences from the same university and PhD in science and geotectonics from the Universidade de São Paulo, Brasil. Sebastián works as a researcher in the Grupo de Investigación en Estratigrafía y Vulcanología (GIEV) Cumanday-Instituto de Investigaciones en Estratigrafía (IIES) at the Universidad

de Caldas and is part of the EGEO research group at the Universidad Nacional Sede Medellín. His main research area is the regional geology and tectonostratigraphic evolution of convergent margins.



Juan Carlos RAMÍREZ is a doctoral candidate at the Universidade de São Paulo working on thermal modeling of the Eastern Cordillera of Colombia and adjacent basins. He received his BS and MS degrees in geology from the Universidad Industrial de Santander. He has worked as a consulting geologist for the oil industry in Colombia, including research topics such as stratigraphy, structural geology, basin analysis, and thermochronology.



Andrés MORA is the technical leader of onshore Colombia and foothills exploration at Ecopetrol. He received his BS in geology from the Universidad Nacional de Colombia and PhD from the Institut für Geowissenschaften, Universität Potsdam. His research interests include structural geology, petroleum exploration, and petroleum geology.



Edward R. SOBEL is the thermochronology professor at the Universität Potsdam. He is responsible for running the thermochronology laboratories, including the fission-track lab and the helium extraction line for (U–Th)/He thermochronology. His research interests focus on constraining deformation and exhumation histories by using multiple thermochronometers combined with geologic, topographic, and climatic data with the aim of understanding the underlying tectonic history and the interactions between tectonic and surface processes. In a larger sense, his research has focused on basin analysis, sedimentology, thermochronology, regional tectonics, and near-surface processes, primarily in the Central Andes and Central Asia.



Ariel ALMENDRAL is a senior research scientist working at the Norwegian Computing Center in Oslo, Norway. His main areas of expertise include stochastic fault/subsurface modeling, history matching, and facies modeling. He holds a PhD from the Universitetet i Oslo in the field of numerical mathematics applied to financial derivatives. He also worked in thermokinematic basin modeling in an earlier position as a consultant for the Instituto Colombiano del Petróleo.



Andrés PARDO-TRUJILLO is a geologist in the Departamento de Ciencias Geológicas at the Universidad de Caldas (Manizales, 1998). Andrés obtained his MS in vegetal micropaleontology in 1997 and his PhD in Science from Liège University (Belgium, 2004). He has worked since 1989 as a professor in the Departamento de Ciencias Geológicas at Universidad de Caldas, Colombia, in sedimentology, regional geology, palynology, and field geology. From 2006–2009, he worked as an advisor at the Agencia Nacional de Hidrocarburos (ANH), where he participated in the geological study of several Colombian sedimentary basins. Andrés is currently the director of the Instituto de Investigaciones en Estratigrafía (IIES) and of the Grupo de Investigación en Estratigrafía y Vulcanología (GIEV) at the Universidad de Caldas. His main interest is the study of the geological and biological evolution of the NW corner of South America during the Cretaceous – Cenozoic.

